Journal for ImmunoTherapy of Cancer

Targeting of GSDMD sensitizes HCC to anti-PD-1 by activating cGAS pathway and downregulating PD-L1 expression

Tingting Lv,[1,2] Xiaofeng Xiong,[3] Wei Yan,[3] Mei Liu,[3] Hongwei Xu,[1] Qin He [1]

To cite: Lv T, Xiong X, Yan W, *et al*. Targeting of GSDMD sensitizes HCC to anti-PD-1 by activating cGAS pathway and downregulating PD-L1 expression. *Journal for ImmunoTherapy of Cancer* 2022;**10**:e004763. doi:10.1136/jitc-2022-004763

► Additional supplemental material is published online only. To view, please visit the journal online (http://dx.doi.org/10.1136/jitc-2022-004763).

Accepted 23 May 2022

[1]Department of Gastroenterology, Shandong Provincial Hospital Affiliated to Shandong First Medical University, Jinan, Shandong, China
[2]Department of Cancer Center, Shandong Provincial Hospital Affiliated to Shandong First Medical University, Jinan, Shandong, China
[3]Tongji Hospital of Tongji Medical College of Huazhong University of Science and Technology, Wuhan, Hubei, China

Correspondence to
Dr Qin He; heqin@sdfmu.edu.cn

ABSTRACT

Background Gasdermin D (GSDMD) is well known as a downstream of inflammasomes. However, the roles of GSDMD itself in hepatocellular carcinoma (HCC) remain unclear.

Methods Two independent cohorts of patients with HCC were analyzed to evaluate the pathological relevance of GSDMD/pTBK1/PD-L1. GSDMD knockout (GSDMD-/-) mice, Alb-Cre mice administered with an adeno-associated virus (AAV) vector that expressed the gasdermin-N domain (AAV9-FLEX-GSDMD-N) and their wild-type littermates were used to induce hepatocarcinogenesis or metastatic HCC. Combination of anti-programmed cell death protein-1 (PD-1) and GSDMD inhibitor dimethyl fumarate (DMF) was used to test for improved therapeutic efficacy. RNA sequencing was used to explore the mechanisms how GSDMD promoted HCC progression.

Results The expression of GSDMD and GSDMD-N was upregulated in HCC tissues or metastatic HCC tissues and positive GSDMD expression indicated grim prognosis. Diethylnitrosamine/carbon tetrachloride or thioacetamide-treated GSDMD-/- mice exhibited decreased liver tumors. In contrast, AAV9-FLEX-GSDMD-N promoted hepatocarcinogenesis. RNA sequencing manifested that knockout of GSDMD impacted the cyclic GMP-AMP synthase (cGAS) pathway and immune-associated pathway. GSDMD damped cGAS activation by promoting autophagy via outputting potassium (K+) and promoted programmed death ligand-1 (PD-L1) expression by histone deacetylases/signal transducer and activator of transcription 1 (STAT1)-induced transactivation of PD-L1 via importing calcium (Ca2+). High Mobility Group Box 1/toll-like receptor 4 (TLR4)/caspase-1 pathway contributed to the overexpression and cleavage of GSDMD. Anti-PD-1 combining with DMF largely impaired HCC progression and metastasis.

Conclusions Targeting GSDMD could promote expression of interferons through inactivation of cGAS pathway and downregulated the PD-L1 expression. Therefore, combined anti-PD-1 and GSDMD inhibitor might serve as an effective treatment option for patients with HCC with GSDMD upregulation.

WHAT IS ALREADY KNOWN ON THIS TOPIC

⇒ Gasdermin D (GSDMD) has been known as a downstream of inflammasomes.
⇒ Checkpoint blockade immunotherapy has limited efficacy in patients with hepatocellular carcinoma (HCC).
⇒ High Mobility Group Box 1 (HMGB1) could cleave pro-caspase-1 and promotes HCC metastasis.

WHAT THIS STUDY ADDS

⇒ Upregulated-GSDMD contributes to hepatocarcinogenesis and indicates poor prognosis.
⇒ GSDMD deficiency ameliorates hepatic tumorigenesis and gasdermin-N domain upregulation promotes hepatic tumorigenesis.
⇒ GSDMD damped cyclic GMP-AMP synthase activation through autophagy by outputting potassium (K^+) and promoted programmed death ligand-1 (PD-L1) expression by histone deacetylases/signal transducer and activator of transcription 1 (STAT1)-induced transactivation of PD-L1 via importing calcium (Ca^{2+}).
⇒ HMGB1/toll-like receptor 4 (TLR4)/caspase-1 pathway contributed to the overexpression and cleavage of GSDMD.
⇒ Combined anti-programmed cell death protein-1 (PD-1) and GSDMD inhibitor might serve as an effective treatment option for patients with HCC with GSDMD upregulation.

HOW THIS STUDY MIGHT AFFECT RESEARCH, PRACTICE AND/OR POLICY

⇒ Combined anti-PD-1 and GSDMD inhibitor might serve as an effective treatment option for patients with HCC with GSDMD upregulation.

INTRODUCTION

Hepatocellular carcinoma (HCC) has been one of the most aggressive malignancies with an increased incidence in the world, and the mortality ranks top two among all the cancer-related deaths worldwide.[1] Although advanced therapeutic options have witnessed substantial progress, the 5-year survival rate of HCC remains low.[2] Recent years, immune-checkpoint inhibitors (ICIs) have made great success in treating cancers including HCC. However, single-agent ICIs provide clinical benefits only in 15%–20% of patients with HCC.[3] Therefore, exploring the driving events involving in HCC progression and microenvironment is of paramount

importance in identifying therapeutic targets and improving the prognosis.

Gasdermin D (GSDMD) is identified as the pyroptosis executioner and could be cleaved to release its gasdermin-N domain (GSDMD-N) via caspase-1 or caspase-11/4/5.[4] GSDMD-N locates in plasma membrane leading to pore formation, cell swelling, massive release of the pro-inflammatory cellular contents, and ion fluxion like potassium efflux and calcium influx.[5–7] GSDMD-induced pyroptosis strengthens the immune defense function.[8] Accumulating evidences have illustrated that GSDMD-induced pyroptosis participates in human diseases like liver fibrosis, non-alcoholic steatohepatitis,[9 10] spinal cord injury[11] and colitis.[12] However, no evidence is currently available on whether GSDMD itself may contribute to HCC progression. Our previous work has reported that inflammation and glutamate exchange facilitate HCC progression.[13] Considering the roles of GSDMD in inflammation and species exchange, we hypothesized that GSDMD could be a new avenue for therapeutic intervention of HCC.

Cyclic GMP-AMP synthase (cGAS) has been discovered as a cytosolic DNA sensor to mount innate immunity and viral defense.[14] Once the activation of cGAS by double-stranded DNA (dsDNA), type I interferons (IFNs) are produced through STING-TBK1-IRF3 pathway.[14] Activation of cGAS-STING in cancer cells functions in restricting tumorigenesis, attenuating tumor growth, and recruiting immune cells for tumor clearance by upregulating inflammatory genes, such as type I IFNs.[15] Therefore, exploring the mechanisms by which cGAS-STING is activated is a promising option for the defense of tumors.

Here, we demonstrated that GSDMD and GSDMD-N were upregulated in HCC and indicated poor prognosis. Knockout of GSDMD impaired hepatocarcinogenesis and upregulating GSDMD-N had the opposite effect. GSDMD-N upregulation inhibited activation of cGAS pathway by promoting the efflux of K^+ and transactivated programmed death ligand-1 (PD-L1) expression by Ca^{2+}/ histone deacetylases (HDACs)/signal transducer and activator of transcription 1 (STAT1) axis. Clinically, patients with HCC with positive expression of GSDMD/PD-L1 had worse prognosis, and positive GSDMD and negative pTBK1 indicated worse outcome. Moreover, High Mobility Group Box 1 (HMGB1)/toll-like receptor 4 (TLR4)/caspase-1 pathway contributed to the upregulation and cleavage of GSDMD. The combined application of GSDMD inhibitor dimethyl fumarate (DMF) and anti-programmed cell death protein-1 (PD-1) abrogated HCC progression.

Materials and methods

Clinical samples

For survival analysis, two independent cohorts of patients with HCC at Tongji hospital of Tongji Medical College (Wuhan, China) were used. The details of the two cohorts were addressed as previously described.[13] In addition, 10 normal liver tissues, 50 pairs of fresh HCC tissues and adjacent non-tumor tissue samples and 30 paired metastatic and matched primary HCC tissues were collected after surgical resection and were used for further investigations.

Animals and animal models

All mice were maintained in animal facilities under standard conditions. C57BL/6J wild-type (WT) mice, *GSDMD*$^{-/-}$ mice, and Alb-Cre mice administered with an adeno-associated virus (AAV) vector that expressed the GSDMD-N (AAV9-FLEX-GSDMD-N) mice were used in this study. Fourteen-day-old *GSDMD*$^{-/-}$, AAV9-GSDMD-N and WT mice administered 25 mg/kg diethylnitrosamine (DEN; Sigma Aldrich) via intraperitoneal (i.p.) injection following the administration of 0.5 µL/g carbon tetrachloride (CCl_4) dissolved in corn oil via i.p. injection once per week for 20 weeks[16] or administration of thioacetamide (TAA) for 40 weeks[17] to induce hepatocarcinogenesis. For the inhibition of GSDMD, the mice were treated with DMF (po, daily, 50 mg/kg).[18] 300 µg anti-PD-1 antibody or isotype antibody (Bio X cell, West Lebanon, New Hampshire, USA) was injected intraperitoneally every 3 days. 20 mg/kg RU320521 was used to inhibit cGAS in vivo. For in vivo signal detection of liver tumor, D-luciferin (PerkinElmer) at 100 mg/kg was injected intraperitoneally into the mice, and bioluminescence was detected using a Lago X optical imaging system (SI Imaging) as previously described.[13] At the end of experiment, the mice were sacrificed, and their serum, kidneys, livers and lungs were dissected and prepared for standard further examinations.

Cell treatment

Established HCC cell lines were seeded in six-well plates and allowed to attach overnight. Then these cells were treated with recombination human HMGB1 (Sigma), and/or ERK, JNK, P38 and PI3K pathway inhibitors.

Statistical analysis

All values were recorded as the mean±SD. All experiments were repeated with three or more independent biological replicates. Statistical significance between the means of two groups was determined using Student's t-tests (normal distribution), Mann-Whitney U tests (abnormal distribution) or Wilcoxon signed-rank test (matched pairs). The statistics of means of multiple groups were performed using one-way analysis of variance (ANOVA) or two-way ANOVA. Immunohistochemical score was analyzed by χ^2 test. The cumulative recurrence and survival curves were shown by the Kaplan-Meier method and the statistical significance was determined by log-rank test. Multivariate analysis was performed by Cox regression analysis. Correlations were performed by using a Pearson correlation test. Statistical analysis was justified as appropriate among all figures. P values<0.05 were considered to be statistically significant. All of the data were triplicated.

Statistical values were calculated with SPSS software (V.20.0) or GraphPad Prism V.8.0 software.

Other materials and methods applied in this research were available in online supplemental material 1.

RESULTS

GSDMD and its cleaved GSDMD-N are upregulated in HCC tissues and indicate grim clinical prognosis

To characterize the importance of GSDMD in HCC, we first evaluated the messenger RNA (mRNA) expression of full-length GSDMD (GSDMD-FL) in liver biopsies from 10 normal liver tissues and 50 paired HCC specimens. HCC tissues displayed an upregulation of *GSDMD* mRNA level compared with non-tumor tissues and normal liver tissues (figure 1A, left). GSDMD-FL and its cleaved production GSDMD-N were elevated in HCC tissues compared with the non-tumor tissues (figure 1A, right). Consistently, immunohistochemistry (IHC) assay was used to show GSDMD expression in two cohorts of HCC tissue microarray. The results demonstrated that staining of GSDMD was stronger in primary HCC tissues than paired non-tumor tissues (figure 1B and online supplemental figure S1A). Furthermore, patients with positive GSDMD expression had shorter overall survival time and higher recurrent rate than those with negative GSDMD expression (figure 1C). Positive GSDMD expression was positively correlated with microvascular invasion, poor differentiation, and high tumor nodule-metastasis (TNM) classification (online supplemental table S1). Multivariate analysis suggested that GSDMD expression was an independent and significant risk factor for recurrence and reduced survival (online supplemental table S2). Metastasis and recurrence have proved to be the main reasons for the poor outcome.[3] Therefore, we then detected the expression of *GSDMD* mRNA in metastatic and non-metastatic HCC tissues or recurrent and non-recurrent HCC tissues. The results indicated the upregulation of GSDMD mRNA in metastatic and recurrent HCC tissues compared with matched groups (figure 1D). Consistently, IHC staining in metastatic and paired HCC tissues revealed the same pattern of changes (figure 1E). Furthermore, western blotting exhibited that GSDMD-N expression in metastatic HCC tissues was higher than paired HCC tissues (figure 1F). We then detected the expression of GSDMD and GSDMD-N in HCC cells. The result showed that the expression of GSDMD and GSDMD-N in HCC cells was higher than normal liver tissues and normal liver cell (online supplemental figure S1B). Considering these observations, GSDMD is a promising prognostic biomarker in patients with HCC.

Deletion of GSDMD impairs hepatocarcinogenesis and overexpression of GSDMD-N promotes hepatic tumorigenesis in mice

To further characterize the effects of GSDMD on HCC in vivo, we first established a classical DEN/CCl_4-induced mouse model of HCC with *GSDMD* knockout (*GSDMD*$^{-/-}$) by using an established protocol for chemically induced carcinogenesis[17] (figure 2A). Compared with WT mice, we had observed decreased histological lesions in *GSDMD*$^{-/-}$ mice (figure 2B). Remarkably, macroscopic liver analysis revealed that *GSDMD*$^{-/-}$ mice developed less and smaller tumors than controls at end time point (figure 2C). To evaluate hepatocyte proliferation in pre-neoplastic surrounding liver tissues, we next measured proliferating cell nuclear antigen (PCNA) expression by IHC. The results exhibited that *GSDMD* deletion could decrease the numbers of PCNA-positive staining in surrounding tissues compared with control groups (figure 2D). It is well documented that DEN could damage DNA,[19 20] we then analyzed γH2AX expression by IHC. Decreased number of γH2AX-positive hepatocytes in *GSDMD*$^{-/-}$ mice was shown compared with WT mice (figure 2E). Since liver fibrosis leads to cirrhosis followed by HCC and CCL_4 is a source for inducing liver fibrosis.[17] Therefore, histological examinations were used to detect liver fibrosis. Masson and Sirius red staining revealed less collagen fibrils in *GSDMD*$^{-/-}$ mice (figure 2F). Immunofluorescence (IF) revealed the same pattern of changes by αSMA staining (figure 2G). We next correlated hepatic *GSDMD* level with pro-fibrotic markers in liver tissue of WT mice after DEN/CCL_4 administration. By doing so, observations that *GSDMD* level correlated with *Col1a1* or *Acta2* level were shown (figure 2H). These results suggest GSDMD might promote HCC development and progression.

Our above works have demonstrated the importance of GSDMD-N in HCC. In order to further study the effects of GSDMD-N on HCC, an additional hepatocarcinogenesis model was used. Alb-Cre mice were treated with the vector AAV9-FLEX-GSDMD-N or the control vector AAV9-FLEX-control (online supplemental figure S2A). H&E staining showed more lesions in mice administered with AAV9-FLEX-GSDMD-N (online supplemental figure S2B). Furthermore, increased tumor number and tumor size were observed in animals with AAV9-FLEX-GSDMD-N (online supplemental figure S2C). Similarly, PCNA or γH2AX-positive hepatocytes were largely elevated in mice with AAV9-FLEX-GSDMD-N (online supplemental figure S2D). IF revealed that GSDMD-N upregulation promoted expression of αSMA (online supplemental figure S2E). The positive correlation analysis between GSDMD level and pro-fibrotic markers was exhibited in online supplemental figure S2F. All of these works demonstrate the importance of GSDMD-N in hepatic tumorigenesis.

GSDMD exerts tumorigenic promotive effects in fibrosis-associated HCC

To strengthen the promotive impacts of GSDMD on HCC in vivo and to further detect its potential effects on fibrosis-associated hepatocarcinogenesis, we next performed another HCC model. TAA was administered to induce fibrosis-associated hepatocarcinogenesis by drinking water,[21] starting at week 8 of age, and animals were harvested 40 weeks post-TAA administration (online supplemental figure S3A). *GSDMD*-deficient animals

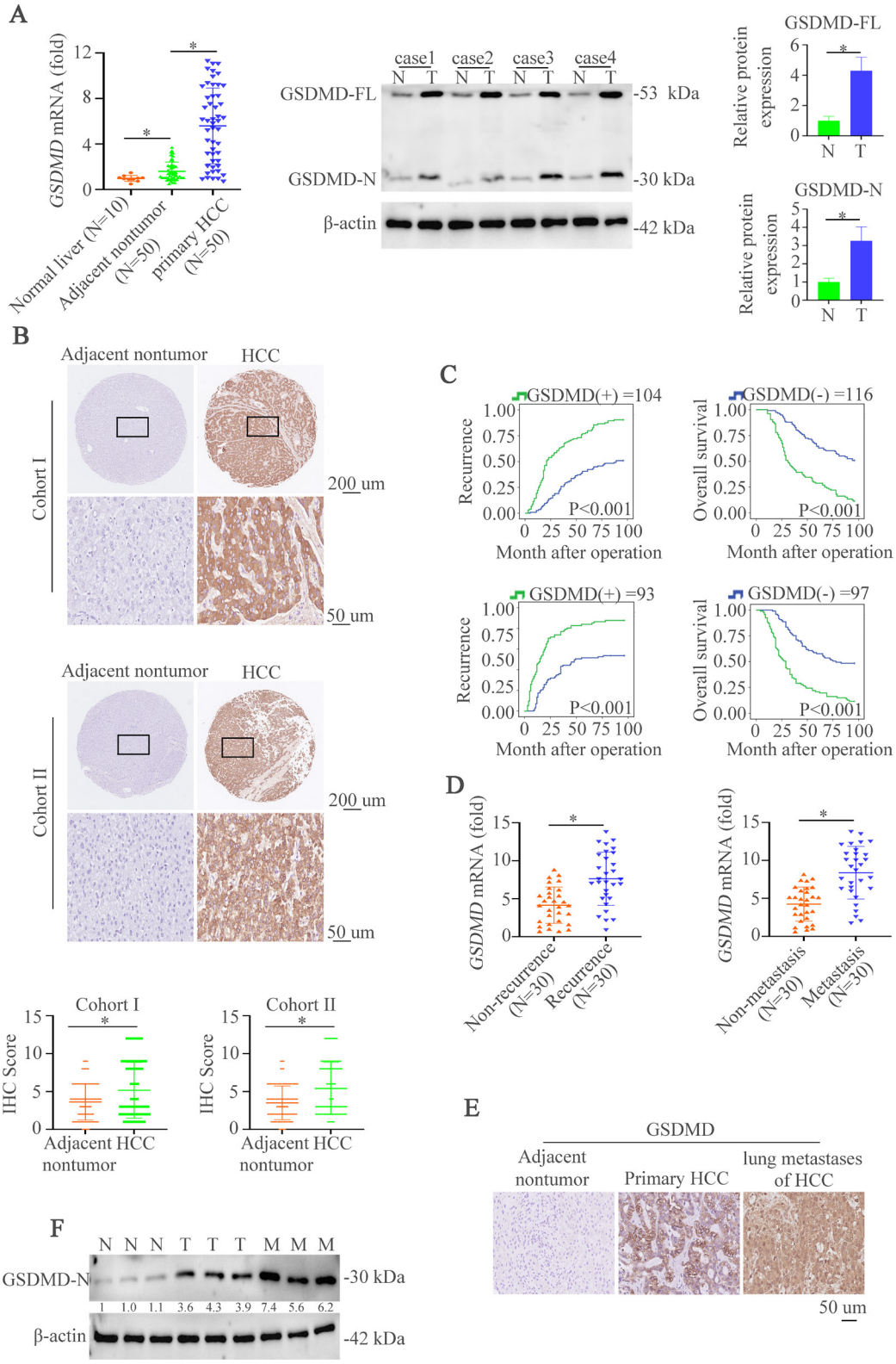

Figure 1 GSDMD and its cleaved GSDMD-N are upregulated in HCC tissues and indicate grim clinical prognosis. (A) RT-qPCR was used to detect GSDMD expression in normal liver tissues (n=10) and 50 paired HCC tissues. Western blotting was applied to detect expression of GSDMD-FL and GSDMD-N expression in paired HCC tissues. (B) Representative IHC images showed GSDMD expression in HCC and adjacent non-tumor tissues in two HCC cohorts. (C) Kaplan-Meier illustrated overall survival time and recurrent rate with positive or negative GSDMD expression in two independent HCC cohorts. (D) RT-qPCR was used to detect GSDMD expression in with or without recurrent patient with HCC samples (n=30) and 30 paired metastatic samples. (E) IHC showed GSDMD expression in adjacent non-tumor, HCC or metastatic tissues. (F) Western blotting exhibited GSDMD-N expression in adjacent non-tumor, HCC or metastatic tissues. GSDMD, gasdermin D; GSDMD-FL, full-length GSDMD; GSDMD-N, gasdermin-N domain; HCC, hepatocellular carcinoma; IHC, immunohistochemistry.

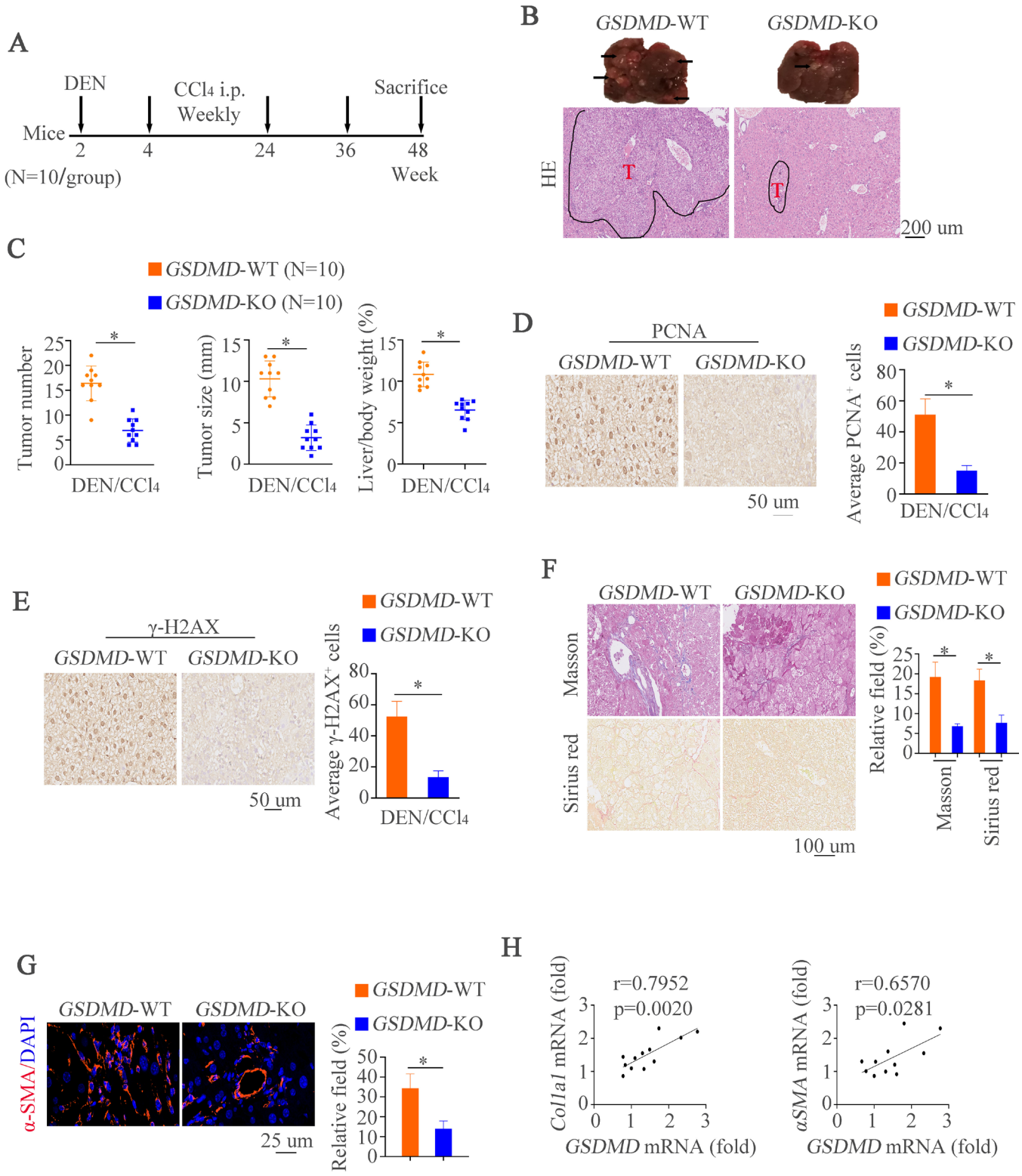

Figure 2 Deletion of GSDMD impairs hepatocarcinogenesis and overexpression of GSDMD-N promotes tumorigenesis in mice. (A) A schematic diagram for procedure of hepatocarcinogenesis induced by DEN and CCL_4. (B) Representative liver and H&E images showed liver tumors of both genotypes at indicated time points. (C) Tumor numbers, maximal size and liver weight of tumors from both groups. (D) Representative IHC images illustrated proliferative hepatocytes at indicated time points measured by PCNA positive nucleus staining. (E) Representative IHC images exhibited damaged hepatocytes at indicated time points measured by γH2AX staining. (F) Masson and Sirius red staining were used to show collagenous fiber in different groups. (G) αSMA staining in liver tissues. (H) Correlation of *GSDMD* mRNA expression with mRNA expression of *Clo1a1* and *ACTA2* in non-tumor areas of hepatic tissues from WT or $GSDMD^{-/-}$ animals treated with DEN and CCl_4. CCl_4, carbon tetrachloride; DEN, diethylnitrosamine; GSDMD, gasdermin D; GSDMD-N, gasdermin-N domain; IHC, immunohistochemistry; mRNA, messenger RNA; PCNA, proliferating cell nuclear antigen; WT, wild type.

exhibited smaller tumors and less tumors number post-TAA versus controls (online supplemental figure S3B-C) and akin to the DEN/CCl_4 model, this was associated with attenuated PCNA and γH2AX$^+$levels (online supplemental figure S3D). Pathological staining shown by Masson and Sirius red demonstrated the decreased fibrosis level (online supplemental figure S3E). IF showed the decreased expression of αSMA (online supplemental figure S3F). The expression of *GSDMD* level was associated with *colla1* or *αSMA* level (online supplemental figure S3G). Taken together, these data encompassing different murine models unequivocally suggests that GSDMD and GSDMD-N promotes HCC tumorigenesis.

GSDMD deficiency promotes the activation of cGAS pathway in HCC

To further dissect the mechanisms by which GSDMD induced HCC progression, we performed RNA sequencing (RNA-seq) analysis by using liver tissues of WT and GSDMD$^{-/-}$ mice with DEN/CCl_4 treatment (online supplemental figure S4A). The Metascape [22]and Kyoto Encyclopedia of Genes and Genomes analysis showed the main changes pathways between WT and *GSDMD*$^{-/-}$ mice (figure 3A–B). One of the top 10 pathways was cytosolic DNA-sensing pathway which promoted type I IFNs.[23] In order to verify whether this pathway was involved in GSDMD-induced HCC, we first detected the downstream genes of cGAS pathway. RT-qPCR analysis verified significantly increased mRNA expression such as IFN-b1 and IFN-a1 associated with cGAS-dependent pathway (figure 3C). The ELISA showed that downregulation of IFN-β and tumor necrosis factor (TNF)-α was found in GSDMD-deficient mice (figure 3D). Next, we used the HCC cells to verify these results. The Huh7 and MHCC97H cells were selected to establish two stable cell lines: Huh7-GSDMD-N upregulating GSDMD-N and MHCC97H-shGSDMD targeting GSDMD (online supplemental figure S1C-E). GSDMD-N upregulation impaired the expression of IFN-β and TNF-α. However, GSDMD downregulation had inverse effects (online supplemental figure S4B).

After binding dsDNA, cGAS promotes the production of the second messenger cGAMP and then binds to STING, which initiates IFN-β transcription by triggering the phosphorylation of TBK1 and IRF3.[14] To explore which step was affected by GSDMD, downstream of cGAS signaling in WT and GSDMD$^{-/-}$ mice was examined. GSDMD knockout induced phosphorylation of STING, TBK1 and IRF3 compared with controls (figure 3E). These results hinted that cGAS activation itself was intended to be affected by GSDMD. After binding DNA, cGAS forms oligomerization which can be visualized by punctate staining.[14 24 25] To define this, IF was used to detect cGAS puncta formation. The puncta were higher in the GSDMD knockout groups than controls (figure 3F). Consistent with oligomerization of cGAS, the quantity of cGAMP in GSDMD-KO group was higher than in WT group (figure 3G). Similarly, GSDMD downregulation in MHCC97H cells also exhibited elevated cGAMP level. However, upregulation of GSDMD-N in Huh7 cells lowered the cGAMP level (online supplemental figure S4C). Furthermore, the non-reducing polyacrylamide gel electrophoresis analysis demonstrated that the number of STING dimers was higher in GSDMD-knockout mice or poly(dA:dT)-treated MHCC97H cells with GSDMD knockdown than controls. However, poly(dA:dT)-treated Huh7 cells with GSDMD-N upregulation exhibited lower STING dimer expression (figure 3H). Taken together, these data illuminates that cGAS is a target of GSDMD which suppresses IFN-β production

GSDMD suppresses cGAS activation and type I IFNs production by promoting autophagy via outputting K$^+$ in HCC

We next defined the mechanisms how GSDMD suppressed cGAS function in HCC. We first tried to analyze whether damaged cells could regulate IFN-β production. Glycine could delay the swelling and rupture of cells and has no effects on membrane pores and metabolic activity.[7 26–28] Therefore, glycine was used to inhibit cell death. Huh7 cells treated with glycine which exhibited resistance to GSDMD-induced decrease of cell vitality, did not produce higher amounts of IFN-β than controls (online supplemental figure S4D). The interleukin (IL)-1β and IL-18 are released via the membrane pores in a GSDMD-dependent manner. Therefore, it is possible that IL-1β and/or IL-18 may regulate the IFN-β production through an autocrine or paracrine fashion. To test this hypothesis, we compared poly(dA:dT)-induced IFN-β production in Huh7 cells with anti-IL-1β or IL-18 treatment. The results showed no significant change on IFN-β release between these groups (online supplemental figure S4E). These results rule out the roles of cell lysis, IL-1β or IL-18 in GSDMD-regulated IFN-β production.

GSDMD-induced forming of membrane pores permit ionic fluxes which are an early event before cell lysis.[7] Recent study demonstrates that ionic perturbations govern cellular functions.[29] Taking all of this into consideration, we hypothesized that ionic fluxes may play a role in GSDMD-induced regulation of cGAS-dependent IFN-β responses. Calcium has been reported to flux across the membrane pores.[30] We first detected the function of calcium in IFN-β responses triggered by GSDMD. The result demonstrated that calcium chelator, BAPTA-AM, had no effect on IFN-β response to cytosolic DNA (online supplemental figure S4F). K$^+$ is the most abundant ion in intracellular milieu, which may cross the plasma membrane. First, we assessed whether GSDMD triggered K$^+$ efflux by using the specific potassium stain, APG4.[31 32] We observed that the intracellular K$^+$ dropped significantly in Huh7-GSDMD-N cells and downregulation of GSDMD inhibited the efflux of K$^+$ (figure 4A). We then detected the K$^+$ efflux under the HCC cells treated with glycine and the result illustrated that K$^+$ efflux was diminished under the presence of glycine (figure 4B). This result might hint that the decrease of intracellular K$^+$ was not due to cell lysis. A study has found that K$^+$ efflux was

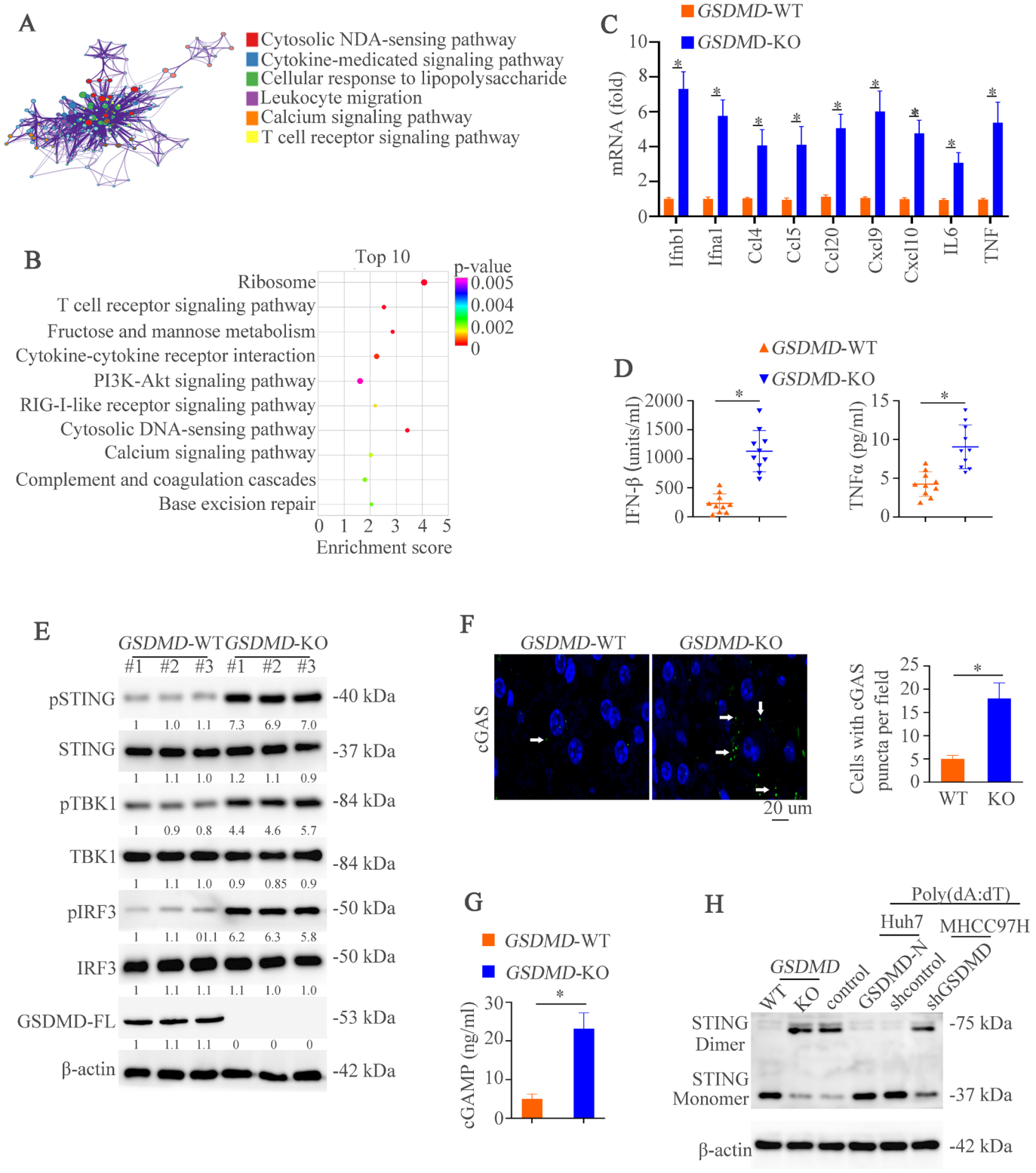

Figure 3 GSDMD deficiency promotes the activation of cGAS pathway in hepatocellular carcinoma. (A) The Metascape analysis stated main changed pathways between WT and GSDMD$^{-/-}$ mice. (B) Top 10 pathways between WT and GSDMD$^{-/-}$ mice were exhibited. (C) RT-qPCR analysis of indicated genes in liver tissues sorted from mice in WT and GSDMD$^{-/-}$ mice. (D) Protein levels of IFN-β and TNF-α was detected by ELISA in different groups. (E) Western blotting was used to analyze phosphorylated (p-)STING, STING, pTBK1, TBK1, pIRF3, IRF3, GSDMD-FL, and β-actin. (F) IF images illustrated punctate staining in different groups. (G) cGAMP amount in WT and GSDMD$^{-/-}$ mice was measured by UPLC/MS analysis. (H) STING monomers and dimers in lysates of WT and GSDMD$^{-/-}$ mice, and Huh7-control, huh7-GSDMD-N, MHCC97H-shcontrol and MHCC97H-shGSDMD stimulated with poly(dA:dT) were assessed by non-reducing polyacrylamide gel electrophoresis and western blotting. cGAS, cyclic GMP-AMP synthase; GSDMD, gasdermin D; GSDMD-FL, full-length GSDMD; IFN, interferon; TNF, tumor necrosis factor; UPLC/MS; ultra performance liquid chromatography/tandem mass spectrometry; WT, wild type.

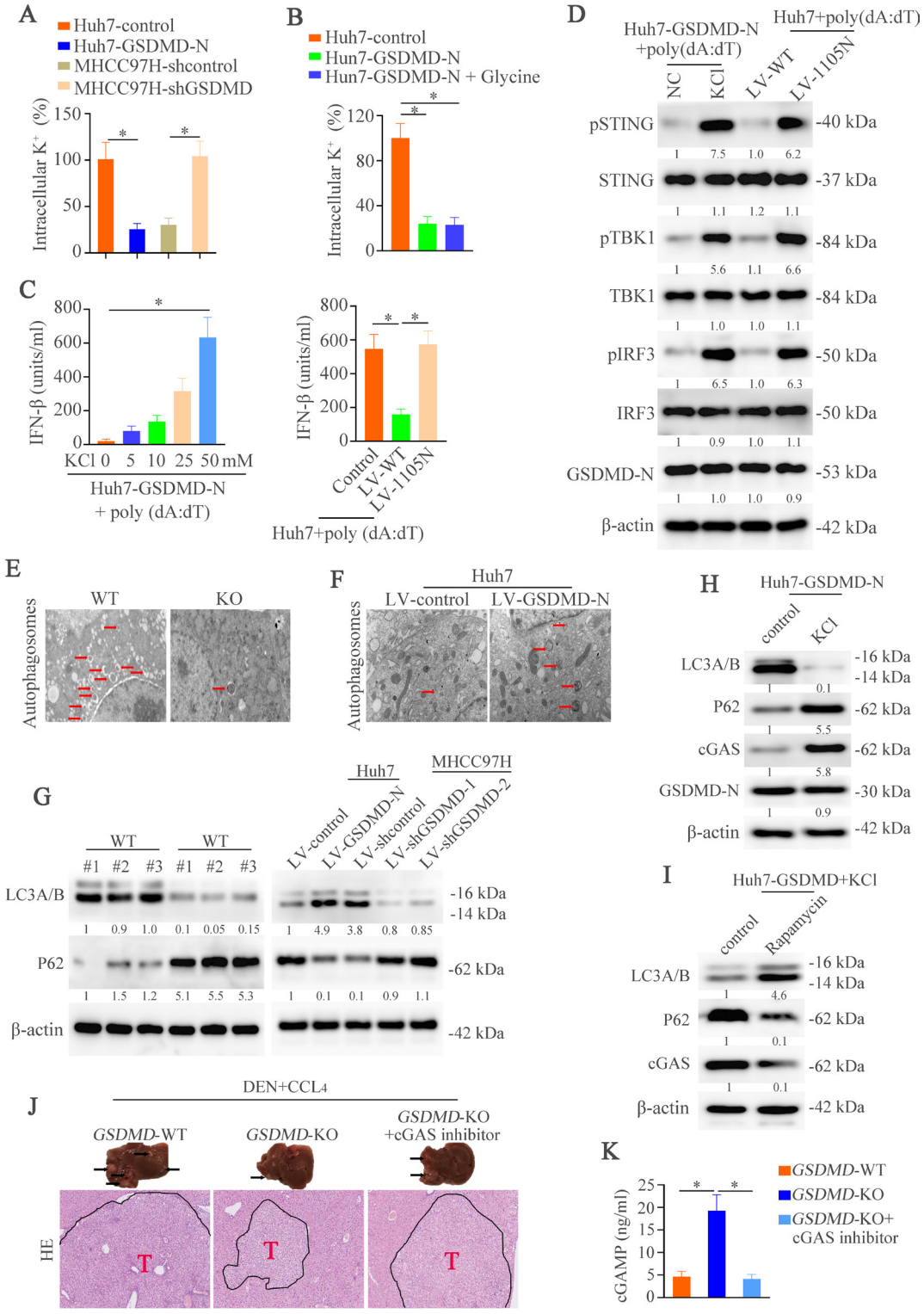

Figure 4 GSDMD promotes output of intracellular K^+ which regulates IFN-β expression via autophagy. (A–B) Intracellular K^+ was assessed by APG4 staining in indicated groups. (C) IFN-β secretion in indicated cell stimulated with poly(dA:dT) was detected by ELISA. (D) Western blotting analyzed pSTING, STING, pTBK1, TBK1, pIRF3, IRF3, GSDMD-N, and β-actin in Huh7-GSDMD-N with or without KCl and Huh7 transfected with LV-WT or LV- I105N stimulated with poly(dA:dT). (E,F) Transmission electron microscope was shown in different groups. (G) Western blotting exhibiting LC3A/B, P62 and β-actin in different groups. (H) Western blotting exhibiting LC3A/B, P62, cGAS and β-actin in Huh7-GSDMD with or without KCl. (I) Western blotting exhibiting LC3A/B, P62, cGAS and β-actin in Huh7-GSDMD with or without Rapamycin. (J) Representative liver and H&E images illustrated liver tumors of three groups at the indicated time points. (J) cGAMP amounts in indicated group mice as measured by UPLC/MS analysis. CCl_4, carbon tetrachloride; cGAS, cyclic GMP-AMP synthase; DEN, diethylnitrosamine; GSDMD, gasdermin D; GSDMD-N, gasdermin-N domain; IFN, interferon; LC3, light chain 3; UPLC/MS, ultra performance liquid chromatography/tandem mass spectrometry; WT, wild type.

inhibited by increasing extracellular concentration of K^+ via adding KCl.[33] We first found that K^+ concentration had no effect on the HCC cell viability (online supplemental figure S4G). We then used the TLR2 ligand Pam3CSK4[34] to stimulate the Huh7-GSDMD cells with or without KCl . The results found that KCl itself might not induce IFN-β after the stimulation of Pam3CSK4 (online supplemental figure S4H). The incubation of poly(dA:dT)-treated Huh7-GSDMD-N cells with increasing concentrations of KCl increased IFN-β secretion (figure 4C left). These works demonstrate that GSDMD attenuates cGAS-induced IFN-β secretion by promoting K^+ efflux. An isoleucine-to-asparagine mutation at position 105 (I105N) in the N terminus of GSDMD compromises its capacity to oligomerize, forming pores and ionic fluxes.[35] We stably transfected Huh7 cells with WT or I105N mutant GSDMD and found that this mutation largely increased IFN-β secretion (figure 4C right). The western blotting also verified that supplement of KCl and transfection of GSDMD with I105N mutant could effectively inactivate the cGAS pathway (figure 4D). All of these results suggest that K^+ efflux is necessary for GSDMD-induced IFN-β secretion.

Researches have reported the connection of cGAS and autophagy,[36 37] and efflux of K^+ could promote the autophagy.[38 39] Furthermore, in the liver tissues, we found the decreased autophagosomes in the $GSDMD^{-/-}$ mice compared with WT mice by transmission electron microscope (TEM) (figure 4E). Therefore, we hypothesized that GSDMD might regulate the cGAS pathway through autophagy. Then, we used HCC cell lines to detect autophagosomes by TEM. We found that overexpression of GSDMD-N increased the number of autophagosomes. However, GSDMD knockdown impaired autophagy (figure 4F). Microtubule-associated protein light chain 3 (LC3) and P62 served as good markers of autophagy process.[40 41] The western blotting exhibited decreased LC3 expression and increased expression of P62 and cGAS under the knockout of GSDMD. The similar results were identified in HCC cell lines (figure 4G). These results indicated that GSDMD might regulate the autophagy.

To further evaluate whether GSDMD increased autophagy through releasing K^+, we supplemented the potassium chloride in Hun7-GSDMD cells. The results demonstrated that K^+ supplement decreased the expression of LC3 and upregulated P62 level. We then detected whether autophagy was involved in cGAS level. In Huh7-GSDMD cells with potassium chloride, autophagy was decreased (figure 4H). However, the autophagy agonist decreased cGAS expression (figure 4I). All of these results illustrated that GSDMD dependent K^+ efflux inhibited activation of cGAS pathway through autophagy.

cGAS inhibitor effectively reverses GSDMD knockout-induced inhibition of hepatic tumorigenesis

To evaluate the importance of cGAS in GSDMD-induced HCC in vivo, we then treated the GSDMD-KO mice with cGAS inhibitor RU320521.[42] Compared with GSDMD-KO mice, we found larger histological lesions when treated with cGAS inhibitor (figure 4J). Macroscopic liver analysis showed more and larger tumors in GSDMD-KO mice treated with cGAS inhibitor (online supplemental figure S5A). GSDMD knockout significantly improved the liver function. In contrast, cGAS inhibitor deteriorated liver function (online supplemental figure S5B). Similarly, we found that cGAMP level was decreased after the cGAS inhibitor treatment (figure 4K), which was consistent with the protein expression of cGAS downstream (online supplemental figure S5C). Finally, the expression of type I IFNs was decreased with cGAS inhibitor (online supplemental figure S5D). These results illustrate that GSDMD might promote HCC development through inhibiting cGAS pathway.

GSDMD upregulates PD-L1 expression through Ca^{2+}/ HDACs / STAT1 pathway

Our above works have demonstrated that T cell receptor signaling pathway was regulated by GSDMD (figure 3A–B). PD-1 is one of the most vital receptors comprised in T cell receptor signaling pathway and PD-L1 is a special ligand which counteracts T cell-activating signals and induces durable tumor progression.[43 44] Our previous study also demonstrates the importance of PD-L1 in HCC metastasis.[13] Therefore, we hypothesized that GSDMD might regulate PD-L1 expression. In both HCC models, we found that GSDMD knockout downregulated PD-L1 expression (figure 5A). Similarly, PD-L1 expression was increased in Huh7-GSDMD-N cells and decreased in MHCC97H-shGSDMD cells compared with control cells in both mRNA and protein levels (figure 5B–C). These data hinted that PD-L1 could be regulated by GSDMD in a transcription-dependent way. In order to verify this premise, we detected *CD274* (encoding PD-L1) promoter activity induced by GSDMD-N through dual-luciferase reporter system. GSDMD-N transfection was markedly increased *CD274* promoter activity (figure 5D). Bioinformatics analysis identified several putative transcription factors binding sites within *CD274* promoter. Through serial deletion mapping and point mutagenesis, we found that STAT1 binding site was essential for GSDMD-N-induced *CD274* promoter activation (figure 5E). In order to further verify this result, we detected the *CD274* promoter activity and found that knockdown of STAT1 impaired promoter activity induced by GSDMD-N overexpression (figure 5F). A chromatin immunoprecipitation (ChIP) assay further confirmed the direct binding of STAT1 to *CD274* promoter (figure 5G). After downregulating STAT1, we observed decreased expression of PD-L1 in both mRNA and protein (figure 5H–I). These results suggest that GSDMD-N promotes the expression of PD-L1 through STAT1.

We then determined to define how GSDMD-N promoted STAT1 to access to *CD274* promoter. Transcription factors binding to gene promoters are dependent on chromosomal structural changes regulated by histones.[45] Therefore, we used the ChIP analysis to assess if epigenetic regulation was occurred in our study. The results

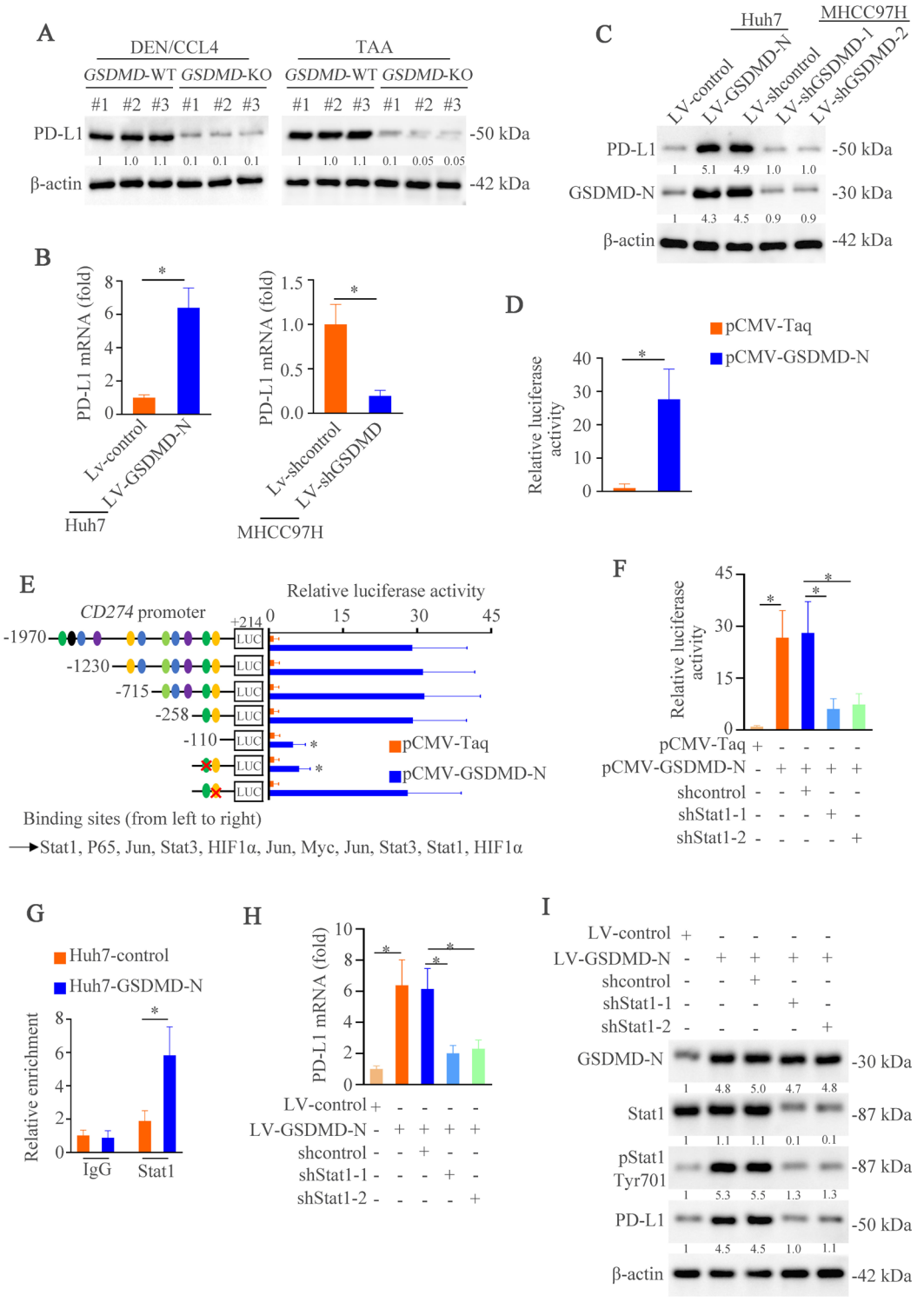

Figure 5 GSDMD upregulates PD-L1 expression through inducing phosphorylation of STAT1. (A) Western blotting analyzed PD-L1 expression in WT and GSDMD$^{-/-}$ group treated with diethylnitrosamine/carbon tetrachloride or thioacetamide. (B) The mRNA expression of PD-L1 in Huh7-control, Huh7-GSDMD-N, MHCC97H-shcontrol and MHCC97H-shGSDMD. (C) The expression of PD-L1 and GSDMD-N in indicated groups was measured by western blotting. (D) *CD274* promoter activity was detected after the overexpression of GSDMD-N in Huh7 cells. (E) Truncated and mutated *CD274* promoter sequences and pCMV-GSDMD-N were cotransfected into Huh7 cells for testing luciferase activity. (F) *CD274* promoter activity was detected after overexpression of GSDMD-N in Huh7 cells transfected with or without shSTAT1. (G) chromatin immunoprecipitation assays showed binding of STAT1 on *CD274* promoter in hepatocellular carcinoma cells. (H) RT-qPCR analysis of PD-L1 mRNA after overexpression of GSDMD-N in Huhn7 cells transfected with or without shSTAT1. (I) Western blotting analyzed STAT1, pSTAT1, PD-L1, GSDMD-N and β-actin after overexpression of GSDMD-N in Huh7 cells transfected with or without shSTAT1. CCL_4, carbon tetrachloride; DEN, diethylnitrosamine; GSDMD, gasdermin D; GASMD-N, gasdermin-N domain; mRNA, messenger RNA; PD-L1, programmed death ligand-1; TAA, thioacetamide.

showed direct binding of H4ac, H3k27ac and H3k9ac to *CD274* promoter under upregulation of GSDMD-N rather than trimethylated (me3) histones: H3K9me3 and H3K27me3 (figure 6A, online supplemental figure 6A). Furthermore, among a panel of inhibitors of HDAC, only Trichostatin A (TSA) and Vorinostat (SAHA) (pan–class I and class II HDAC inhibitors) as well as Entinostat (MS-275) (selective class I HDAC inhibitor) rather than other inhibitors promoted PD-L1 mRNA level (figure 6B). The ChIP assays further confirmed direct binding of HDACs especially HDAC1 to *CD274* promoter (figure 6C). These findings demonstrate that GSDMD might epigenetically regulate histones acetylation, which promotes the binding of STAT1to PD-L1 promoter and induces PD-L1 transcription.

Next, we determined to find out how GSDMD regulated HDACs. In the figure 3A–B, we found that calcium signaling pathway was regulated by GSDMD and researches have demonstrated that Ca^{2+} could regulate HDACs pathway through calmodulin.[46] Therefore, we first detected the Ca^{2+} influx. The data showed the increase of Ca^{2+} influx in the Huh7-GSDMD-N cells compared with the controls (figure 6D). Calmodulin binds Ca^{2+} with high affinity and directs itself subcellular distribution.[47] Therefore, IF was performed to detect the location of calmodulin. The results exhibited that GSDMD-N upregulation promoted massive nuclear translocation of calmodulin (figure 6E). Furthermore, as determined by coimmunoprecipitation, activated calmodulin bound to HDAC1 at *CD274* promoter (figure 6F). Calcium chelator, BAPTA-AM, decreased the expression of PD-L1 induced by GSDMD-N/STAT1 pathway (figure 6G, online supplemental figure S6B). These results suggest that GSDMD-N upregulation-induced calcium influx promotes nuclear translocation and activation of calmodulin, which in turn removes HDACs from *CD274* promoter and opens chromatin for STAT1 binding and *CD274* transcription.

According to above works, we found that two target genes were involved in GSDMD-induced hepatic tumorigenesis. The decreased release of IFN-β induced tumor progression and upregulation of PD-L1 promoted immune evasion of tumors. Therefore, we thought both of them play an important role in hepatic tumorigenesis. In order to verify this hypothesis, we performed subcutaneous xenograft mice model. The mice were treated with phosphate buffered saline, IFN-β or IgG, anti-PD-L1 by intratumor injection. The results showed that IFN-β overexpression and anti-PD-L1 treatment decreased tumor growth (online supplemental figure S6C,D). IHC staining for Ki67 in xenografts exhibited lowered proliferation of tumor cells induced by IFN-β injection and anti-PD-L1 treatment (online supplemental figure S6E). Although the results showed that the anti-PD-L1 treatment lowered the tumor growth more than IFN-β under the basis of measurements, there were no statistically significant values. Therefore, we conclude that both target genes had important roles in GSDMD-induced hepatic tumorigenesis.

GSDMD expression is positively associated with PD-L1 expression and negatively associated with pTBK1 expression in human HCC tissues

We above work demonstrated that GSDMD could regulate the expression of pTBK1 and PD-L1 and then we profiled the expression of pTBK1 and PD-L1 by IHC staining in two independent HCC cohorts. Representative IHC images of GSDMD, pTBK1 and PD-L1 expression were shown in online supplemental figure 7A. IHC score found that GSDMD expression was positively associated with PD-L1 upregulation. However, GSDMD expression was negatively associated with pTBK1 in both HCC cohorts (online supplemental figure 7B). Our previous work has found that positive PD-L1 expression indicated poor prognosis.[13] In contrast, HCC tissues with positive pTBK1 displayed a lower aggressive tumor phenotype (online supplemental table S3) and were associated with a better prognosis (online supplemental figure 7C). Furthermore, patients with co-expression of GSDMD/PD-L1 had the worse prognosis (online supplemental figure 7D). However, patients with positive GSDMD and negative pTBK1 expression had the worse prognosis (online supplemental figure 7E).

HMGB1 contributes to GSDMD-FL upregulation through TLR4/ERK/P65 pathway and cleaves GSDMD-FL through activating caspase-1

The molecular mechanism of GSDMD-FL upregulation in HCC is still unclear. Several studies have found that caspase-1 could cleave GSDMD-FL into GSDMD-N[5] and HMGB1 could promote caspase-1 activation.[48] Therefore, we assumed that HMGB1 might induce GSDMD upregulation and cleave c-terminal in HCC. To verify this hypothesis, we first cultured Huh7 cells with recombinant human HMGB1. RT-qPCR and western blotting demonstrated that HMGB1 stimulated expression of GSDMD-FL and GSDMD-N in a dose-dependent manner (figure 7A and online supplemental figure 8A). These results demonstrate that HMGB1 could promote transcription and cleave GSDMD-FL.

To decipher how HMGB1 stimulated GSDMD-FL expression, we first found that HMGB1 treatment enhanced *GSDMD* promoter activity (online supplemental figure 8B). We constructed a serial of reporter gene plasmids with truncated and mutated *GSDMD* promoter fragments. A deletion from −521 to −107 bp significantly decreased HMGB1-induced *GSDMD* promoter activity, suggesting that this region was crucial for HMGB1-induced *GSDMD* promoter activation. One presumptive P65 and STAT1, two specificity protein 1 binding sites in this sequence were identified. Mutation of P65 binding site largely impaired HMGB1-mediated *GSDMD* promoter activation whereas mutation of other binding sites in this sequence had little effect (figure 7B). In order to further verify the importance of P65 in HMGB1-induced GSDMD transcription, promoter activity was measured. P65 knockdown impaired promoter activity and mRNA expression of GSDMD induced by HMGB1(online supplemental figure

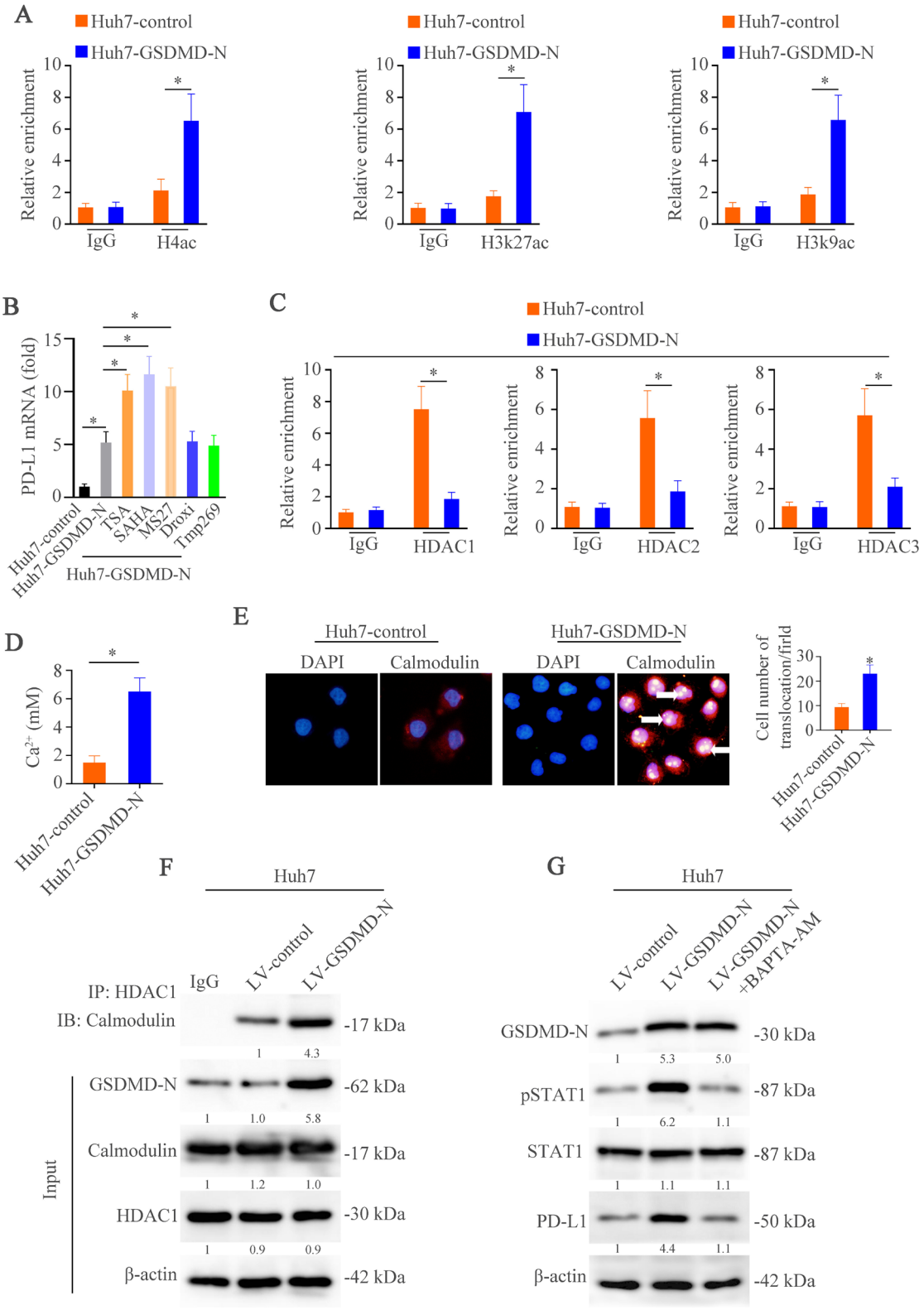

Figure 6 GSDMD upregulates PD-L1 expression through Ca^{2+}/HDACs/STAT1 pathway. (A) ChIP assays were used to illustrate binding of H4ac, H3K27ac and H3K9ac on *CD274* promoter in HCC cells. (B) RT-qPCR analysis of PD-L1 mRNA in the Huh7-control, Huh7-GSDMD-N and Huh7-GSDMD-N with inhibitors of HDACs. (C) The binding of HDAC1, HDAC2 and HDAC3 on *CD274* promoter in HCC cells was detected by ChIP. (D) The Ca^{2+} level was measured in Huh7-control and Huh7-GSDMD-N cells. (E) Immunofluorescence was used to detect calmodulin translocation in Huh7-control and Huh7-GSDMD-N cells. (F) Co-IP was used to show interact of HDAC1 and calmodulin in Huh7-control and Huh7-GSDMD-N cells. (G) Western blotting analyzed STAT1, pSTAT1, PD-L1, GSDMD-N and β-actin in indicated HCC cells. ChIP, chromatin immunoprecipitation; GSDMD, gasdermin D; GSDMD-N, gasdermin-N domain; HCC, hepatocellular carcinoma; HDAC, histone deacetylase; mRNA, messenger RNA; PD-L1, programmed death ligand-1.

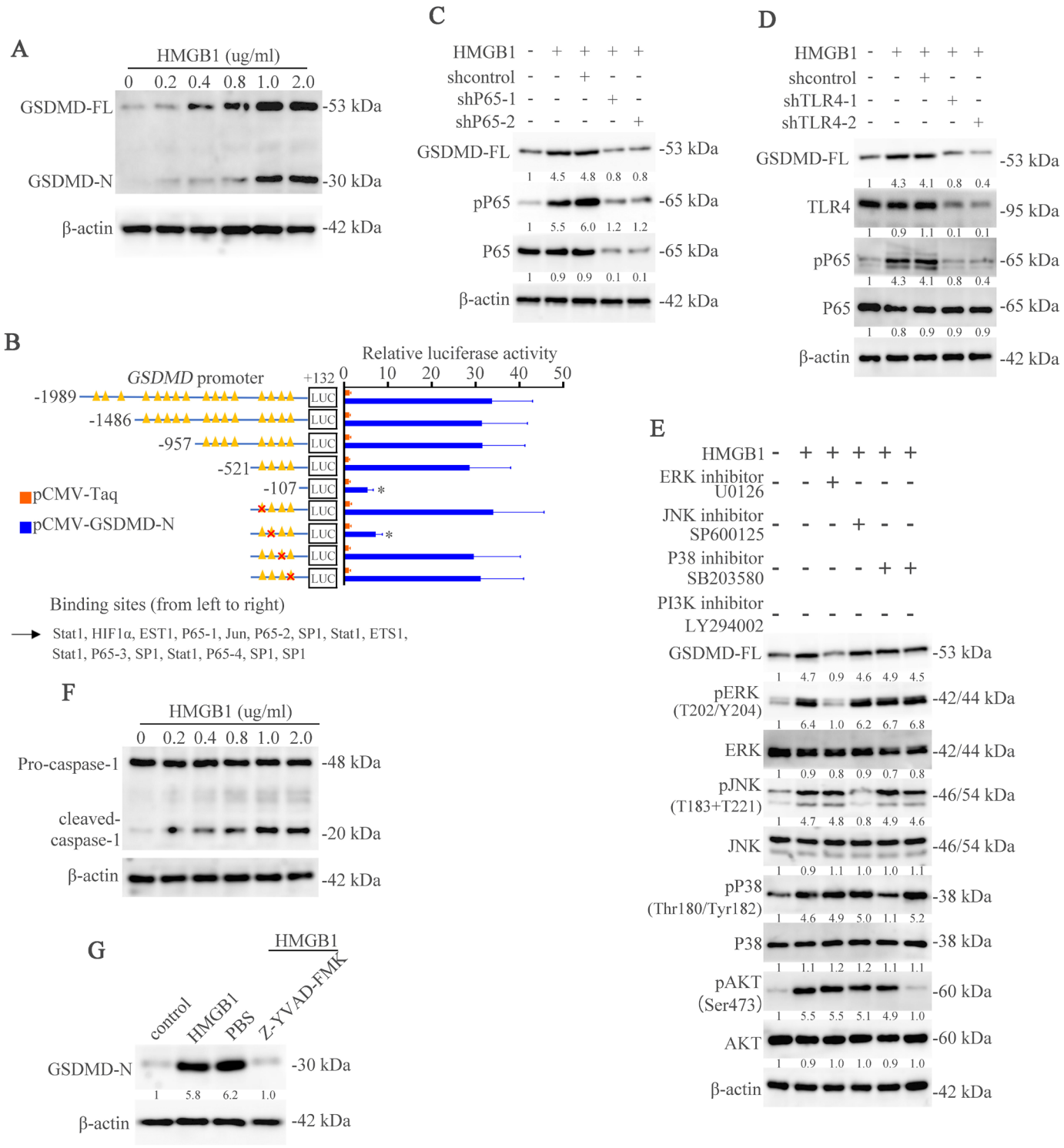

Figure 7 HMGB1 contributes to GSDMD-FL upregulation through TLR4/ERK/P65 pathway and cleaves GSDMD-FL through activating caspase-1. (A) Huh7 cells were treated with recombinant human HMGB1 for 24 hours. GSDMD expression was detected by western blotting. (B) Truncated and mutated *GSDMD* promoter sequences in Huh7 cells transfected with plasmids of shcontrol or shP65 under HMGB1 treatment. (C) Western blotting analyzed P65, pP65, GSDMD-FL and β-actin in indicated HCC cells. (D) Western blotting analyzed TLR4, P65, pP65, GSDMD-FL and β-actin in indicated HCC cells. (E) ERK, JNK, p38, or PI3K pathway inhibitors were applied in Huh7 cells under HMGB1 treatment. Expression of GSDMD-FL, total and phosphorylated ERK, JNK, p38, and AKT was detected by western blotting. (F) Caspase-1 was detected in Huh7 cells treated with HMGB1 by western blotting. (G) GSDMD-N was detected in Huh7 cells treated with HMGB1 and/or Z-YVAD-FMK. GSDMD, gasdermin D; GSDMD-FL, full-length GSDMD; HCC, hepatocellular carcinoma; HMGB1, High Mobility Group Box 1; TLR4, toll-like receptor 4.

S8C,D). The ChIP assay verified that binding of P65 and GSDMD promoter was decreased under P65 knockdown (online supplemental figure 8E). The western blotting showed that P65 knockdown decreased HMGB1-induced GSDMD-FL expression (figure 7C). HMGB1 has been proved to activate the signaling pathway through TLR2, TLR4 and Rage.[49] Therefore, we then determined to detect which receptor was involved in GSDMD-FL expression. We found that only knockdown of TLR4 but not TLR2 and Rage impaired GSDMD-FL expression treated by HMGB1 (figure 7D and online supplemental figure S6F). Several pathways including ERK, JNK, P38 and PI3K have been activated by HMGB1. Which pathway contributed to HMGB1-induced GSDMD-FL expression was unclear. In order to address this question, we treated Huh7 cells with pathway inhibitors under the treatment of HMGB1, the results showed that block of ERK pathway largely abolished the GSDMD-FL expression. All of these data demonstrated that HMGB1 contributes to GSDMD-FL expression through TLR4/ERK/P65 pathway (figure 7E). Our above works also found that HMGB1 could cleave GSDMD-FL to form GSDMD-N (figure 7A). Therefore, we then tried to find how HMGB1 promoted the cleavage of GSDMD-FL. Researches have illustrated that HMGB1 might activate caspase-1 which could induce formation of GSDMD-N. Accordingly, we hypothesized that HMGB1-caspase-1 pathway contributed to the cleavage of GSDMD-FL. The western blotting showed that HMGB1 activated caspase-1 in a dose-dependent manner (figure 7F). Caspase-1 inhibitor Z-YVAD-FMK impaired GSDMN-N expression (figure 7G). These above results suggest that HMGB1 promotes cleavage of GSDMD-FL through activating caspase-1.

To investigate whether HMGB1/GSDMD axia could promote HCC tumorigenesis in mouse models. We performed subcutaneous xenograft mice model to study the role of HMGB1/GSDMD pathway on tumorigenesis. The results showed that HMGB1 increased tumor growth, whereas GSDMD inhibition suppressed tumor growth (online supplemental figure S8F,G). IHC staining for Ki67 in xenografts showed increased proliferation of tumor cells induced by HMGB1, which was reversed by GSDMD knockdown (online supplemental figure S8H). In the vitro, we found that HMGB1 could promote GSDMD expression and impaired the expression of cGAS. In order to confirm these results in clinical specimens, we used IHC staining for detecting HMGB1, cleaved caspase-1, GSDMD, pSTAT1, IFN-β and CD8 expression. Representative IHC images were shown in online supplemental figure S8I. The results found that the expression of HMGB1, cleaved caspase-1 and pSTAT1 was positively associated with GSDMD upregulation, and IFN-β and CD8 expression were negatively associated with GSDMD upregulation. These results illustrated the importance of HMGB1/GSDMD in hepatic tumorigenesis.

Combined treatment of GSDMD inhibitor DMF and anti-PD-1 abolishes hepatic tumorigenesis and HCC metastasis

According to the above works, we hypothesized that block of GSDMD could promote IFN-β production and impair PD-L1 expression, which induced HCC cells death and improved the function and amount of $CD8^+$ T cells. DMF is proved to react with GSDMD and prevent GSDMD interaction with caspases, limiting its processing, oligomerization, and capacity to induce cell death.[18] The downregulation of PD-L1 might improve anti-PD-1 therapy.[43] Therefore, we assumed that combination of GSDMD inhibitor DMF and anti-PD-1 could block HCC tumorigenesis and metastasis through improving IFN-β production and immunosuppressive microenvironment. The sketch of design was shown in online supplemental figure S9A. Bioluminescent images found effectiveness of combination treatment in blocking hepatic tumor progression (figure 8A, online supplemental figure S9B). No significant changes in average mice body weight or toxicity in liver and kidney were observed (online supplemental figure S9C). H&E staining also verified that combined therapeutic pattern strikingly decreased HCC number and size (figure 8B,C). Decreased lung metastasis burden also validated the efficiency of combined therapy (figure 8D). The combination treatment also prolonged survival time of mice (online supplemental figure S9D). To characterize the mechanism under this combination, we examined infiltration of $CD8^+$ T cells in HCC tumors. The combination treatment dramatically increased $CD8^+$ T cells infiltration compared with control group or single agent alone shown by flow cytometer (figure 8E). The results illustrated that combination treatment promoted infiltration and activation of $CD8^+$ T cells, and decreased the number of myeloid-derived suppressor cells (MDSCs) and regulatory T cells (Tregs) (figure 8F, online supplemental figure S9E-G). These results suggest that double blockade of GSDMD and PD-1 improves antitumor immune response and inhibits HCC tumorigenesis and metastasis.

DISCUSSION

HCC is most common in liver cancer and accounts for one of the most cancer-associated deaths. Though understanding of pathophysiology and oncogenes of this disease has improved, this knowledge is yet to be translated into clinical practice. Dominant mutational drivers in HCC, such as *TERT*, *TP53* and *CTNNB1*, remain undruggable.[3] Therefore, finding druggable targets that contributes to HCC progression is urgent.

Pyroptosis is a caspase-1 dependent form of cell death, which is morphologically and mechanistically distinct from other forms of cell death[50] and participates in host defense and human diseases including HCC.[51] GSDMD is discovered to have pore-forming activity and is well studied as effector for pyroptosis.[5] However, the roles of GSDMD itself in HCC remain unclear. Considering the importance of inflammation in HCC, we hypothesized

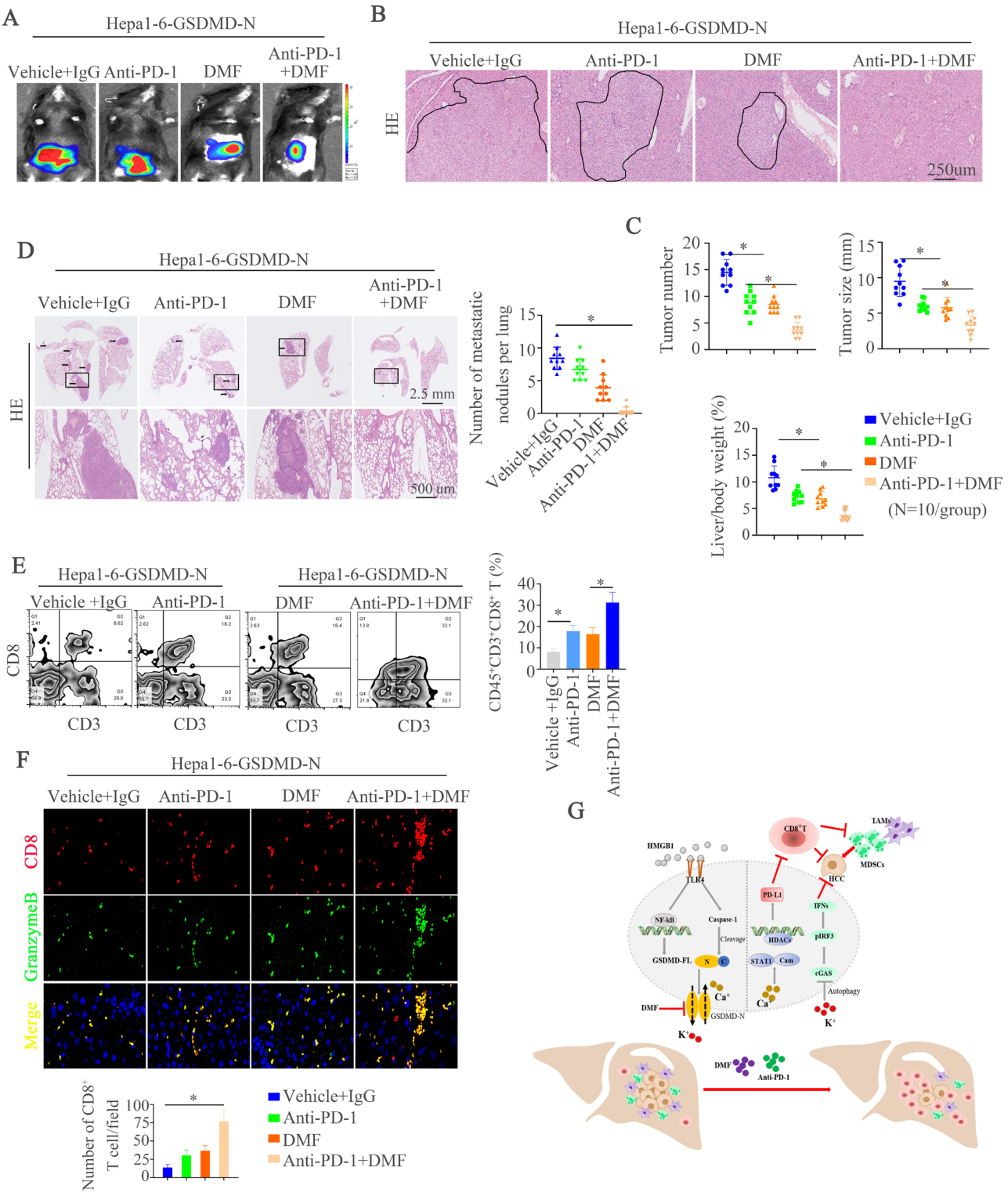

Figure 8 Combined GSDMD inhibitor DMF and PD-1 treatment abolishes hepatic tumorigenesis and HCC metastasis. (A) Representative bioluminescent images in mice liver. (B) Representative H&E images showed liver tumors of different groups at indicated time points. (C) Tumor numbers, maximal size and liver weight of tumors from both groups. (D) H&E staining of metastatic lung nodules was shown in different groups at indicated time points. (E) flow cytometer for $CD8^+$ T cells in HCC tissues of HCC model after indicated treatment was displayed. (F) Immunofluorescence showed infiltration and activation of $CD8^+$ T cells in different groups. (G) A schematic illustration elaborated the role of GSDMD on HCC metastasis. HMGB1 upregulated GSDMD expression through the ERK/P65 pathway. GSDMD overexpression inactivated cGAS pathway and induced programmed death ligand-1 expression through K^+ influx and Ca^{2+} efflux respectively. The combined treatment of anti-PD-1 and GSDMD inhibitor DMF suppressed GSDMD-induced HCC metastasis. cGAS, cyclic GMP-AMP synthase; DMF, dimethyl fumarate; GSDMD, gasdermin D; GSDMD-N, gasdermin-N domain; HCC, hepatocellular carcinoma; HMGB1, High Mobility Group Box 1; PD-1, programmed cell death protein-1.

that GSDMD might induce HCC progression. In this study, we found that GSDMD-FL and GSDMD-N were elevated in HCC especially in metastatic HCC tissues. Positive GSDMD-FL indicated poor outcome and might be an independent biomarker.

cGAS pathway detects intracellular double strand DNA and triggers an innate immune reaction to promote product of type I IFN response which functions in infection, autoimmunity, sterile inflammatory responses and cellular senescence.[52] In this study, we found that GSDMD formed membrane pore and induced efflux of K^+ which blocked cGAS activation and induced IFN-β production. Autophagy in this study was found to connect K^+ and cGAS activation. Nowadays, works reveal that cGAS presents in nucleus and plasma membrane, and such subcellular compartmentalization, which is linked to regulate DNA repair, to activate nuclear factor kappa B subunit 1 (NF-κB) and mitogen activated kinase-like protein (MAPK) pathway and to induce autophagy and lysosome-dependent cell death.[52] Further works should focus on these new roles in human diseases.

PD-L1 is ligand of PD-1 and is a major co-inhibitory checkpoint signaling that controls T cells activity. Blocking PD-L1/PD-1 pathway has consistently shown remarkable antitumor effects in patients with advanced cancers. However, this response rates remain low in HCC.[53] Therefore, exploring regulatory mechanisms that PD-L1 could bring substantial benefits to patients who receive immune treatment is important. In this study, we found importance of GSDMD in regulating PD-L1 expression. Mechanically, we showed that GSDMD promoted Ca^{2+} influx and induced binding of pSTAT1 in PD-L1 promoter. Meanwhile, Ca^{2+} influx induced interacting of calmodulin and HDACs, which promoted pSTAT1 to access into PD-L1 promoter. These works demonstrated the role of GSDMD in regulating PD-L1 expression. Clinically, we found that GSDMD expression was positively associated with PD-L1 expression and negatively associated with pTBK1 expression in human HCC tissues.

In order to find upstream that induced GSDMD-FL expression and cleavage, we focused on HMGB1 which induces HCC progression.[54 55] HMGB1 is reported to activate caspase-1[48] that can induce cleavage of GSDMD-FL. Therefore, we hypothesized HMGB1 might be an upstream of GSDMD upregulation in HCC. Actually, we found that HMGB1 contributed to GSDMD-FL expression through ERK/P65 pathway and cleaved GSDMD-FL into GSDMD-N through caspase-1. Finally, we determined to find therapeutic approaches targeting GSDMD-induced HCC progression. The combined GSDMD-N inhibitor and anti-PD-1 effectively blocked GSDMD-induced HCC progression and metastasis through changing microenvironment and promoting HCC cell death. In conclusion, we demonstrated that HMGB1-induced expression and cleavage of GSDMD promoted HCC tumorigenesis through blocking cGAS pathway and upregulating PD-L1 expression. Treatment of GSDMD inhibitor and anti-PD-1 is a promising approach in abolishing hepatocarcinogenesis and HCC metastasis.

In conclusion, in this study, we identified oncogenic role of GSDMD in HCC. The regulation of GSDMD indicated poor prognosis and GSDMD promoted hepatic tumorigenesis. Mechanically, GSDMD upregulation activated cGAS pathway through K^+ efflux and induced PD-L1 expression through Ca^{2+}/HDACs/STAT1 pathway. Clinically, GSDMD expression was positively associated with PD-L1 expression and negatively associated with pTBK1 expression in human HCC tissues. Furthermore, HMGB1/TLR4/ERK/P65 pathway contributed to GSDMD-FL upregulation and cleaved GSDMD-FL through activating caspase-1. Finally, we found that combined treatment of DMF and anti-PD-1 abolished hepatic tumorigenesis and HCC metastasis.

Contributors TL performed the experiments. XX provided assistance in immunohistochemistry, HE staining, plasmid construction, and animal experiments. WY, ML and HX provided assistance in collecting tissue samples, clinical statistical analysis, and analyzing data. QH designed the study and wrote the paper.

Funding This work was supported by Clinical Science and Technology Innovation Program of Jinan (202134039), National Natural Science Foundation of China (81472311) and Incubation Fund of Shandong Provincial Hospital (2021FY014). We acknowledge the patients who agreed to participate in this clinical trial, as forward trajectory of science hinges on their support. And we also thank the Metascape for help.[55]

Competing interests None declared.

Patient consent for publication Not applicable.

Ethics approval This study involving human studies using liver tissue samples was approved by Shandong Provincial Hospital Affiliated to Shandong First Medical University 2021-571. Participants gave informed consent to participate in the study before taking part.

Provenance and peer review Not commissioned; externally peer reviewed.

Data availability statement All data relevant to the study are included in the article or uploaded as supplementary information.

ORCID iD

Qin He http://orcid.org/0000-0002-9887-9388

REFERENCES

1 Siegel RL, Miller KD, Fuchs HE, *et al*. Cancer statistics, 2021. *CA Cancer J Clin* 2021;71:7–33.
2 Kelley RK, Greten TF. Hepatocellular Carcinoma - Origins and Outcomes. *N Engl J Med* 2021;385:280–2.
3 Llovet JM, Kelley RK, Villanueva A, *et al*. Hepatocellular carcinoma. *Nat Rev Dis Primers* 2021;7:6.
4 Shi J, Gao W, Shao F. Pyroptosis: gasdermin-mediated programmed necrotic cell death. *Trends Biochem Sci* 2017;42:245–54.
5 Shi J, Zhao Y, Wang K, *et al*. Cleavage of GSDMD by inflammatory caspases determines pyroptotic cell death. *Nature* 2015;526:660–5.

6 He W-ting, Wan H, Hu L, *et al*. Gasdermin D is an executor of pyroptosis and required for interleukin-1β secretion. *Cell Res* 2015;25:1285–98.
7 Banerjee I, Behl B, Mendonca M, *et al*. Gasdermin D restrains type I interferon response to cytosolic DNA by disrupting ionic homeostasis. *Immunity* 2018;49:413–26.
8 Miao EA, Leaf IA, Treuting PM, *et al*. Caspase-1-induced pyroptosis is an innate immune effector mechanism against intracellular bacteria. *Nat Immunol* 2010;11:1136–42.
9 Gaul S, Leszczynska A, Alegre F, *et al*. Hepatocyte pyroptosis and release of inflammasome particles induce stellate cell activation and liver fibrosis. *J Hepatol* 2021;74:156–67.
10 Xu B, Jiang M, Chu Y, *et al*. Gasdermin D plays a key role as a pyroptosis executor of non-alcoholic steatohepatitis in humans and mice. *J Hepatol* 2018;68:773–82.
11 Xu S, Wang J, Zhong J, *et al*. CD73 alleviates GSDMD-mediated microglia pyroptosis in spinal cord injury through PI3K/AKT/Foxo1 signaling. *Clin Transl Med* 2021;11:e269.
12 Ma C, Yang D, Wang B, *et al*. Gasdermin D in macrophages restrains colitis by controlling cGAS-mediated inflammation. *Sci Adv* 2020;6:eaaz6717.
13 He Q, Liu M, Huang W, *et al*. IL-1β-Induced Elevation of Solute Carrier Family 7 Member 11 Promotes Hepatocellular Carcinoma Metastasis Through Up-regulating Programmed Death Ligand 1 and Colony-Stimulating Factor 1. *Hepatology* 2021;74:3174–93.
14 Sun L, Wu J, Du F, *et al*. Cyclic GMP-AMP synthase is a cytosolic DNA sensor that activates the type I interferon pathway. *Science* 2013;339:786–91.
15 Kwon J, Bakhoum SF. The cytosolic DNA-Sensing cGAS-STING pathway in cancer. *Cancer Discov* 2020;10:26–39.
16 Sun H, Chen L, Zhou W, *et al*. The protective role of hydrogen-rich saline in experimental liver injury in mice. *J Hepatol* 2011;54:471–80.
17 Esparza-Baquer A, Labiano I, Sharif O, *et al*. TREM-2 defends the liver against hepatocellular carcinoma through multifactorial protective mechanisms. *Gut* 2021;70:1345–61.
18 Humphries F, Shmuel-Galia L, Ketelut-Carneiro N, *et al*. Succination inactivates gasdermin D and blocks pyroptosis. *Science* 2020;369:1633–7.
19 Li M, Lu Y, Li Y, *et al*. Transketolase deficiency protects the liver from DNA damage by increasing levels of ribose 5-phosphate and nucleotides. *Cancer Res* 2019;79:3689–701.
20 Guedj A, Volman Y, Geiger-Maor A, *et al*. Gut microbiota shape 'inflamm-ageing' cytokines and account for age-dependent decline in DNA damage repair. *Gut* 2020;69:1064–75.
21 Brown ZJ, Heinrich B, Greten TF. Mouse models of hepatocellular carcinoma: an overview and highlights for immunotherapy research. *Nat Rev Gastroenterol Hepatol* 2018;15:536–54.
22 Zhou Y, Zhou B, Pache L, *et al*. Metascape provides a biologist-oriented resource for the analysis of systems-level datasets. *Nat Commun* 2019;10:1523.
23 Zhang X, Bai X-C, Chen ZJ. Structures and mechanisms in the cGAS-STING innate immunity pathway. *Immunity* 2020;53:43–53.
24 Cui Y, Yu H, Zheng X, *et al*. SENP7 potentiates cGAS activation by relieving SUMO-Mediated inhibition of cytosolic DNA sensing. *PLoS Pathog* 2017;13:e1006156.
25 Xia P, Ye B, Wang S, *et al*. Glutamylation of the DNA sensor cGAS regulates its binding and synthase activity in antiviral immunity. *Nat Immunol* 2016;17:369–78.
26 Conos SA, Chen KW, De Nardo D, *et al*. Active MLKL triggers the NLRP3 inflammasome in a cell-intrinsic manner. *Proc Natl Acad Sci U S A* 2017;114:E961–9.
27 Evavold CL, Ruan J, Tan Y, *et al*. The pore-forming protein gasdermin D regulates interleukin-1 secretion from living macrophages. *Immunity* 2018;48:35–44.
28 Russo HM, Rathkey J, Boyd-Tressler A, *et al*. Active caspase-1 induces plasma membrane pores that precede pyroptotic lysis and are blocked by lanthanides. *J Immunol* 2016;197:1353–67.
29 Gong Y-N, Guy C, Olauson H, *et al*. ESCRT-Iii acts downstream of MLKL to regulate Necroptotic cell death and its consequences. *Cell* 2017;169:286–300. e16.
30 Geng J, Shi Y, Zhang J, *et al*. TLR4 signalling via Piezo1 engages and enhances the macrophage mediated host response during bacterial infection. *Nat Commun* 2021;12:3519.
31 Eil R, Vodnala SK, Clever D, *et al*. Ionic immune suppression within the tumour microenvironment limits T cell effector function. *Nature* 2016;537:539–43.
32 Prindle A, Liu J, Asally M, *et al*. Ion channels enable electrical communication in bacterial communities. *Nature* 2015;527:59–63.
33 Muñoz-Planillo R, Kuffa P, Martínez-Colón G, *et al*. K(+) efflux is the common trigger of NLRP3 inflammasome activation by bacterial toxins and particulate matter. *Immunity* 2013;38:1142–53.
34 Mukherjee A, Roy S, Patidar A, *et al*. TLR2 dimer-specific ligands selectively activate protein kinase C isoforms in Leishmania infection. *Immunology* 2021;164:318–31.
35 Aglietti RA, Estevez A, Gupta A, *et al*. GsdmD p30 elicited by caspase-11 during pyroptosis forms pores in membranes. *Proc Natl Acad Sci U S A* 2016;113:7858–63.
36 Prabakaran T, Bodda C, Krapp C, *et al*. Attenuation of cGAS-STING signaling is mediated by a p62/SQSTM1-dependent autophagy pathway activated by TBK1. *Embo J* 2018;37. doi:10.15252/embj.201797858. [Epub ahead of print: 13 04 2018].
37 Chen M, Meng Q, Qin Y, *et al*. TRIM14 inhibits cGAS degradation mediated by selective autophagy receptor p62 to promote innate immune responses. *Mol Cell* 2016;64:105–19.
38 Vodnala SK, Eil R, Kishton RJ, *et al*. T cell stemness and dysfunction in tumors are triggered by a common mechanism. *Science* 2019;363. doi:10.1126/science.aau0135. [Epub ahead of print: 29 03 2019].
39 Zhu M, Cao L, Xiong S, *et al*. Na+/K+-ATPase-dependent autophagy protects brain against ischemic injury. *Sig Transduct Target Ther* 2020;5:55.
40 Kuma A, Matsui M, Mizushima N. LC3, an autophagosome marker, can be incorporated into protein aggregates independent of autophagy: caution in the interpretation of LC3 localization. *Autophagy* 2007;3:323–8.
41 Johansen T, Lamark T. Selective autophagy mediated by autophagic adapter proteins. *Autophagy* 2011;7:279–96.
42 Vincent J, Adura C, Gao P, *et al*. Small molecule inhibition of cGAS reduces interferon expression in primary macrophages from autoimmune mice. *Nat Commun* 2017;8:750.
43 Chen DS, Mellman I. Elements of cancer immunity and the cancer-immune set point. *Nature* 2017;541:321–30.
44 Sun C, Mezzadra R, Schumacher TN. Regulation and function of the PD-L1 checkpoint. *Immunity* 2018;48:434–52.
45 Soufi A, Garcia MF, Jaroszewicz A, *et al*. Pioneer transcription factors target partial DNA motifs on nucleosomes to initiate reprogramming. *Cell* 2015;161:555–68.
46 Huang D, Chen J, Yang L, *et al*. NKILA lncRNA promotes tumor immune evasion by sensitizing T cells to activation-induced cell death. *Nat Immunol* 2018;19:1112–25.
47 Chin D, Means AR. Calmodulin: a prototypical calcium sensor. *Trends Cell Biol* 2000;10:322–8.
48 Yan W, Chang Y, Liang X, *et al*. High-mobility group box 1 activates caspase-1 and promotes hepatocellular carcinoma invasiveness and metastases. *Hepatology* 2012;55:1863–75.
49 Andersson U, Tracey KJ. HMGB1 is a therapeutic target for sterile inflammation and infection. *Annu Rev Immunol* 2011;29:139–62.
50 Bergsbaken T, Fink SL, Cookson BT. Pyroptosis: host cell death and inflammation. *Nat Rev Microbiol* 2009;7:99–109.
51 Kist M, Vucic D. Cell death pathways: intricate connections and disease implications. *Embo J* 2021;40:e106700.
52 Hopfner K-P, Hornung V. Molecular mechanisms and cellular functions of cGAS-STING signalling. *Nat Rev Mol Cell Biol* 2020;21:501–21.
53 Cha J-H, Chan L-C, Li C-W, *et al*. Mechanisms controlling PD-L1 expression in cancer. *Mol Cell* 2019;76:359–70.
54 Ye L, Zhang Q, Cheng Y, *et al*. Tumor-derived exosomal HMGB1 fosters hepatocellular carcinoma immune evasion by promoting TIM-1^{+} regulatory B cell expansion. *J Immunother Cancer* 2018;6:145.
55 Liu Y, Yan W, Tohme S, *et al*. Hypoxia induced HMGB1 and mitochondrial DNA interactions mediate tumor growth in hepatocellular carcinoma through Toll-like receptor 9. *J Hepatol* 2015;63:114–21.

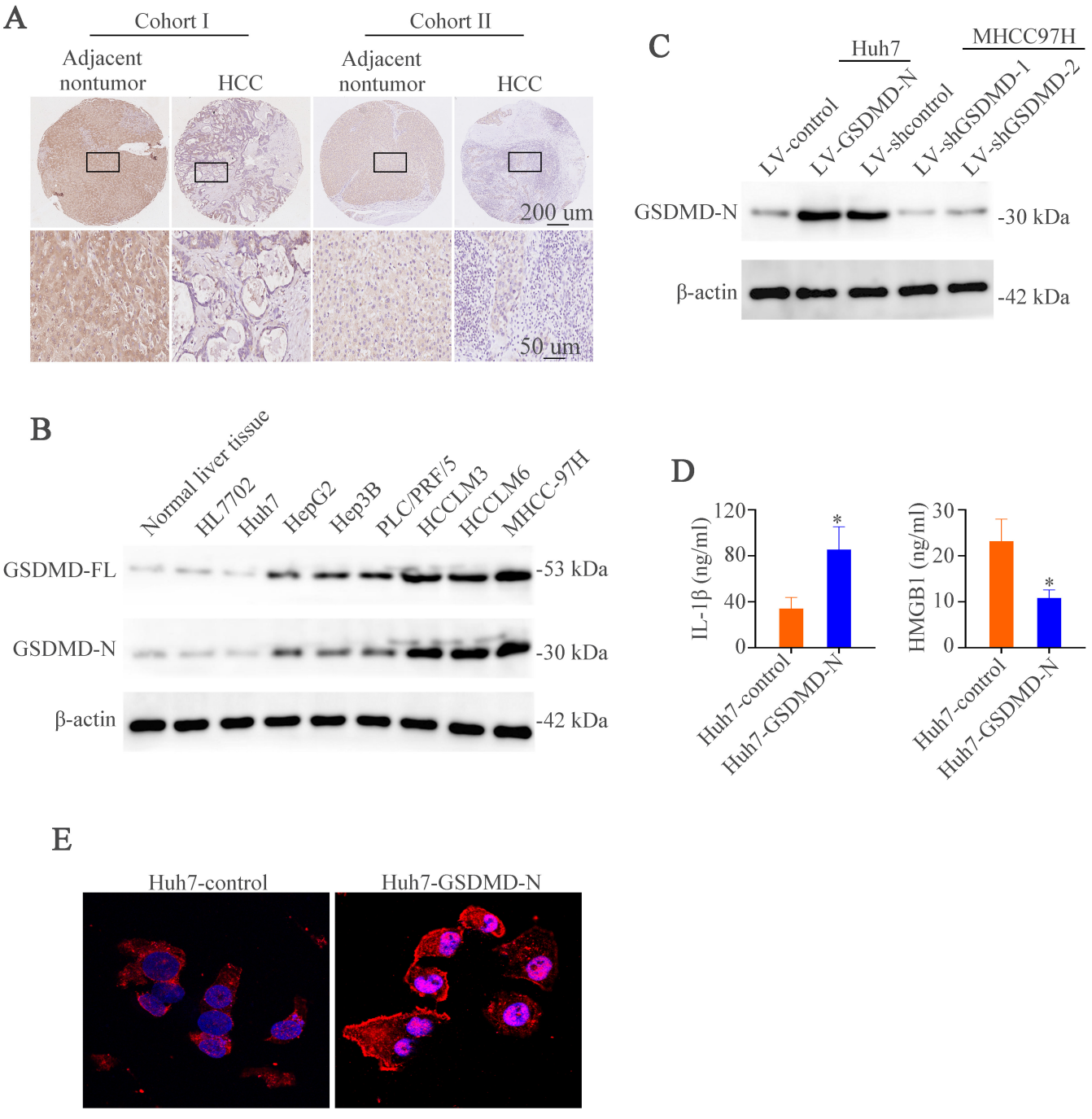
A
Cohort I
Cohort II
Adjacent nontumor
HCC
Adjacent nontumor
HCC
200 um
50 um
B
Normal liver tissue
HL7702
Huh7
HepG2
Hep3B
PLC/PRF/5
HCCLM3
HCCLM6
MHCC-97H
GSDMD-FL
-53 kDa
GSDMD-N
-30 kDa
β-actin
-42 kDa
C
Huh7
MHCC97H
LV-control
LV-GSDMD-N
LV-shcontrol
LV-shGSDMD-1
LV-shGSDMD-2
GSDMD-N
-30 kDa
β-actin
-42 kDa
D
IL-1β (ng/ml)
120
80
40
0
*
Huh7-control
Huh7-GSDMD-N
HMGB1 (ng/ml)
30
20
10
0
*
Huh7-control
Huh7-GSDMD-N
E
Huh7-control
Huh7-GSDMD-N

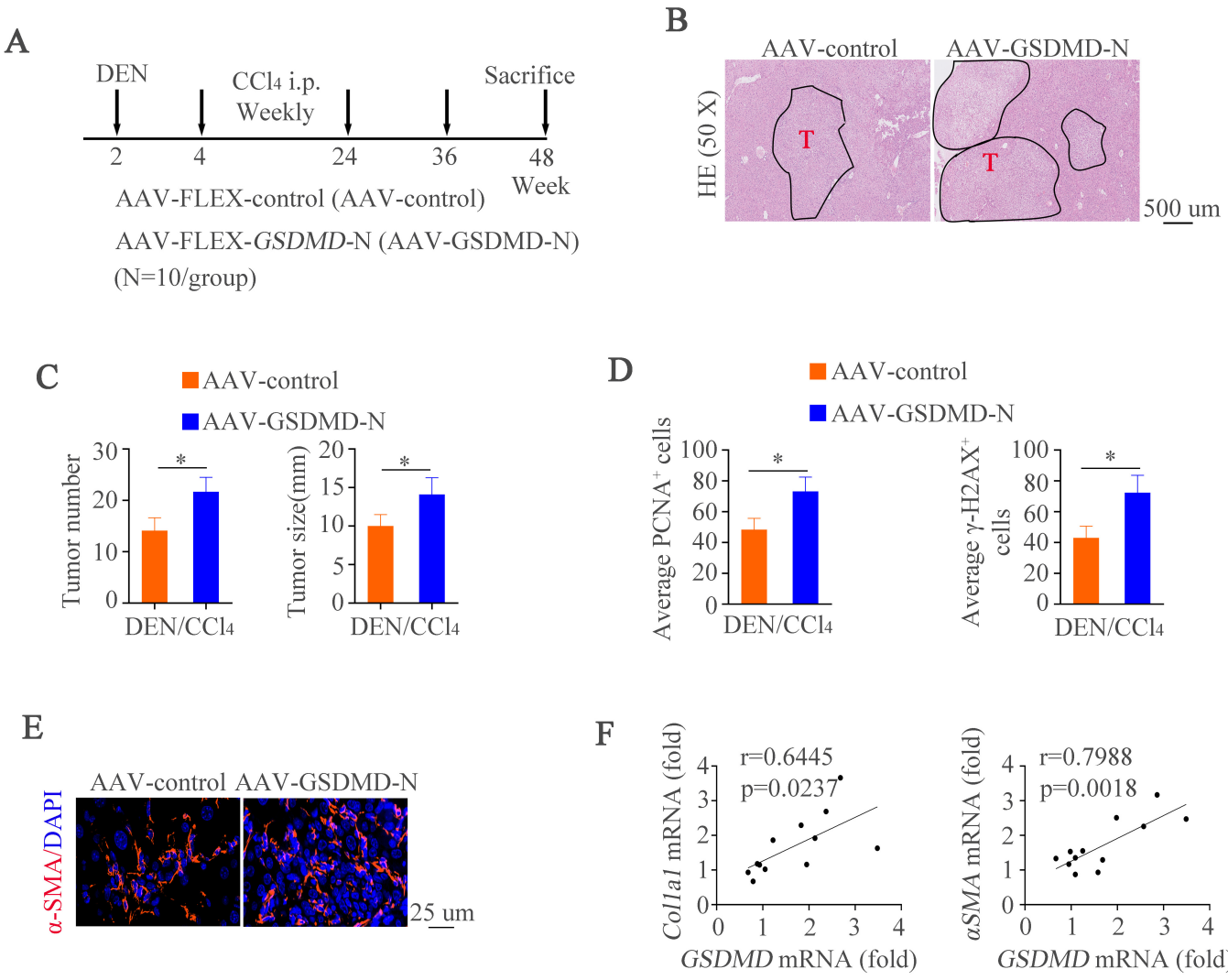
A
DEN
CCl4 i.p.
Weekly
Sacrifice
2
4
24
36
48
Week
AAV-FLEX-control (AAV-control)
AAV-FLEX-GSDMD-N (AAV-GSDMD-N)
(N=10/group)
B
AAV-control
AAV-GSDMD-N
HE (50 X)
T
T
500 um
C
AAV-control
AAV-GSDMD-N
Tumor number
Tumor size(mm)
DEN/CCl4
DEN/CCl4
D
AAV-control
AAV-GSDMD-N
Average PCNA+ cells
Average γ-H2AX+ cells
DEN/CCl4
DEN/CCl4
E
AAV-control AAV-GSDMD-N
α-SMA/DAPI
25 um
F
r=0.6445
p=0.0237
Col1a1 mRNA (fold)
GSDMD mRNA (fold)
r=0.7988
p=0.0018
αSMA mRNA (fold)
GSDMD mRNA (fold)

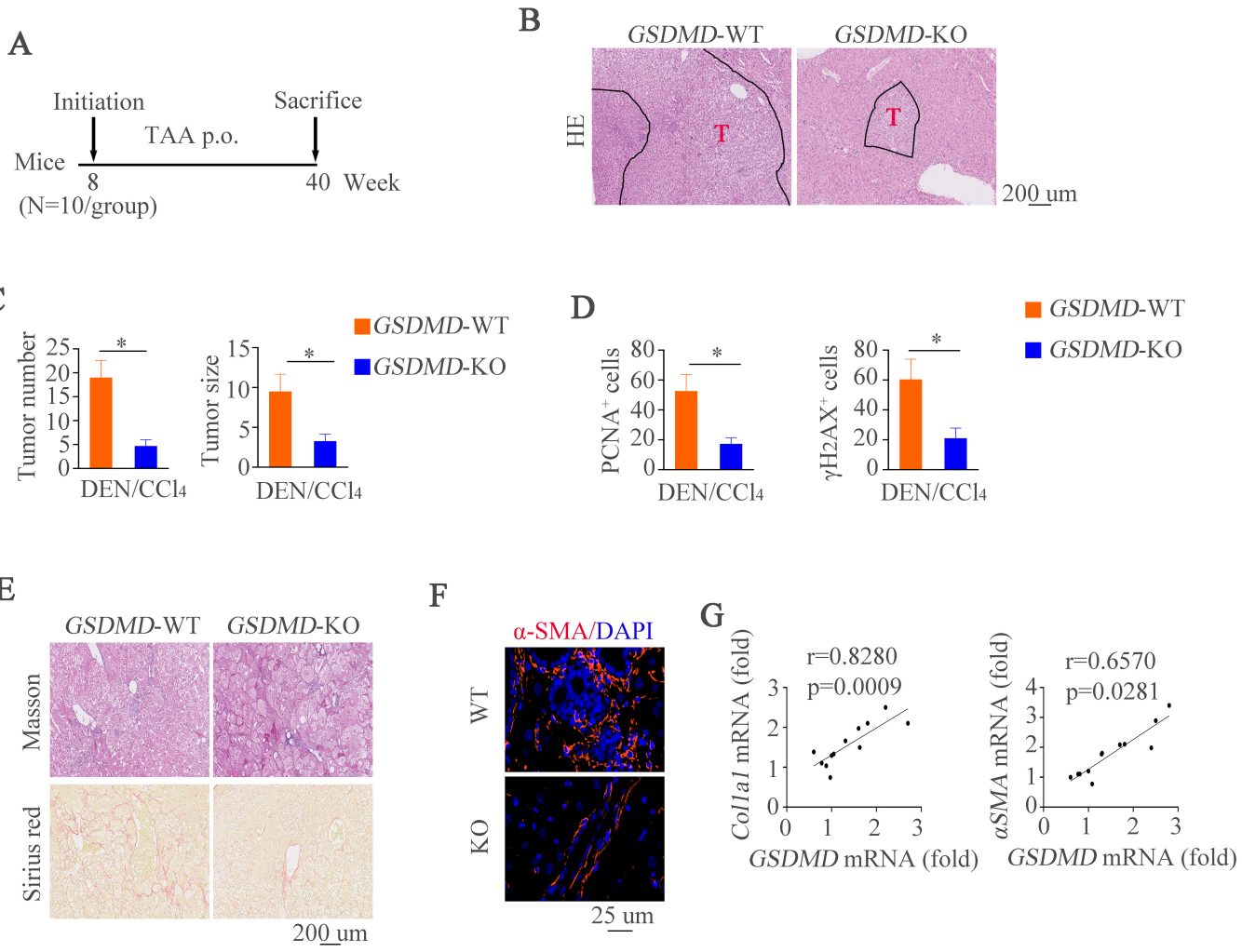
A
Initiation
Sacrifice
TAA p.o.
Mice
8
40 Week
(N=10/group)
B
GSDMD-WT
GSDMD-KO
HE
T
T
200 um
C
Tumor number
Tumor size
GSDMD-WT
GSDMD-KO
DEN/CCl4
DEN/CCl4
D
PCNA+ cells
γH2AX+ cells
GSDMD-WT
GSDMD-KO
DEN/CCl4
DEN/CCl4
E
GSDMD-WT
GSDMD-KO
Masson
Sirius red
200 um
F
α-SMA/DAPI
WT
KO
25 um
G
Col1a1 mRNA (fold)
r=0.8280
p=0.0009
GSDMD mRNA (fold)
αSMA mRNA (fold)
r=0.6570
p=0.0281
GSDMD mRNA (fold)

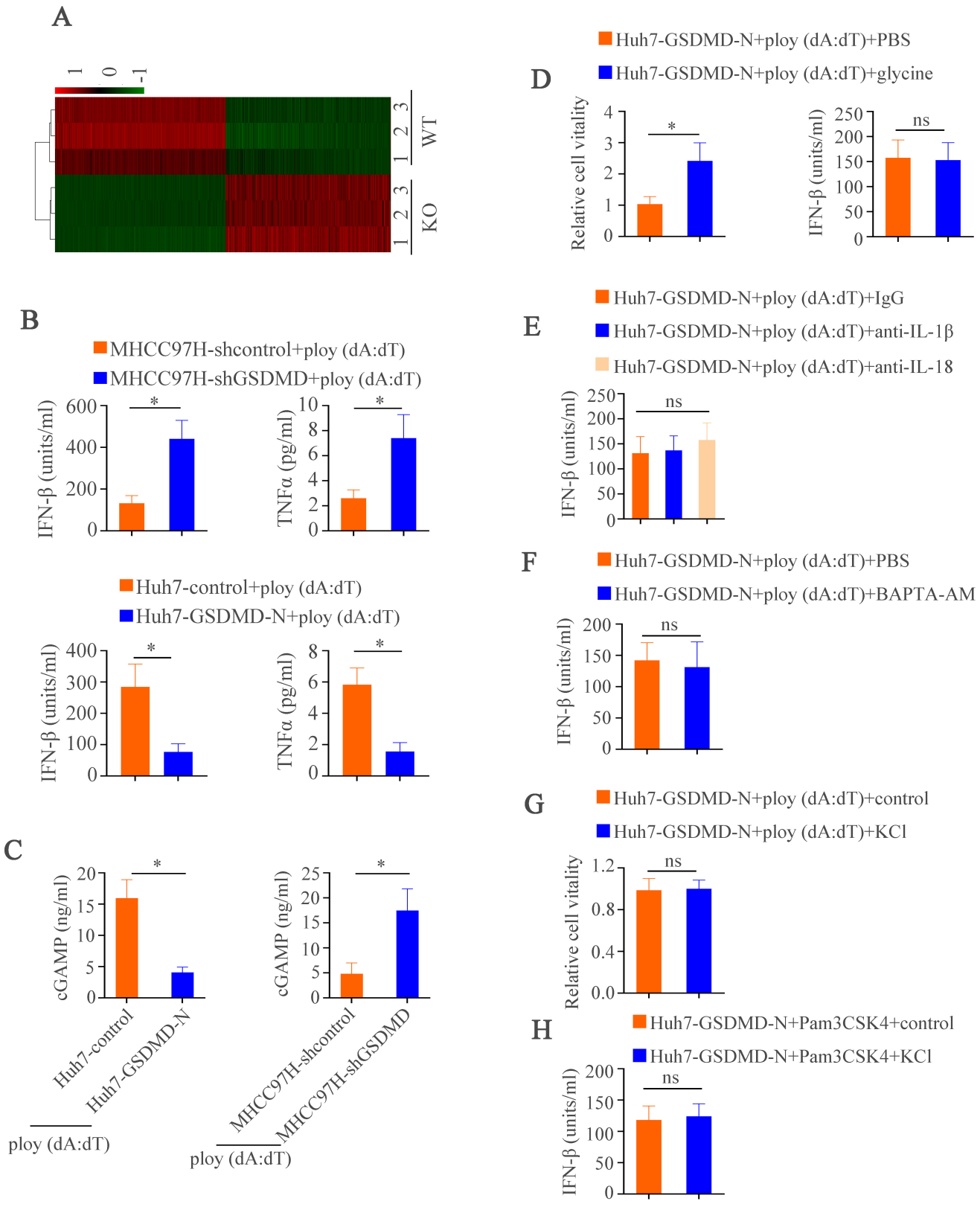
A
1
0
-1
WT
KO
B
MHCC97H-shcontrol+ploy (dA:dT)
MHCC97H-shGSDMD+ploy (dA:dT)
IFN-β (units/ml)
TNFα (pg/ml)
Huh7-control+ploy (dA:dT)
Huh7-GSDMD-N+ploy (dA:dT)
C
cGAMP (ng/ml)
Huh7-control
Huh7-GSDMD-N
ploy (dA:dT)
MHCC97H-shcontrol
MHCC97H-shGSDMD
ploy (dA:dT)
D
Huh7-GSDMD-N+ploy (dA:dT)+PBS
Huh7-GSDMD-N+ploy (dA:dT)+glycine
Relative cell vitality
IFN-β (units/ml)
ns
E
Huh7-GSDMD-N+ploy (dA:dT)+IgG
Huh7-GSDMD-N+ploy (dA:dT)+anti-IL-1β
Huh7-GSDMD-N+ploy (dA:dT)+anti-IL-18
IFN-β (units/ml)
ns
F
Huh7-GSDMD-N+ploy (dA:dT)+PBS
Huh7-GSDMD-N+ploy (dA:dT)+BAPTA-AM
IFN-β (units/ml)
ns
G
Huh7-GSDMD-N+ploy (dA:dT)+control
Huh7-GSDMD-N+ploy (dA:dT)+KCl
Relative cell vitality
ns
H
Huh7-GSDMD-N+Pam3CSK4+control
Huh7-GSDMD-N+Pam3CSK4+KCl
IFN-β (units/ml)
ns

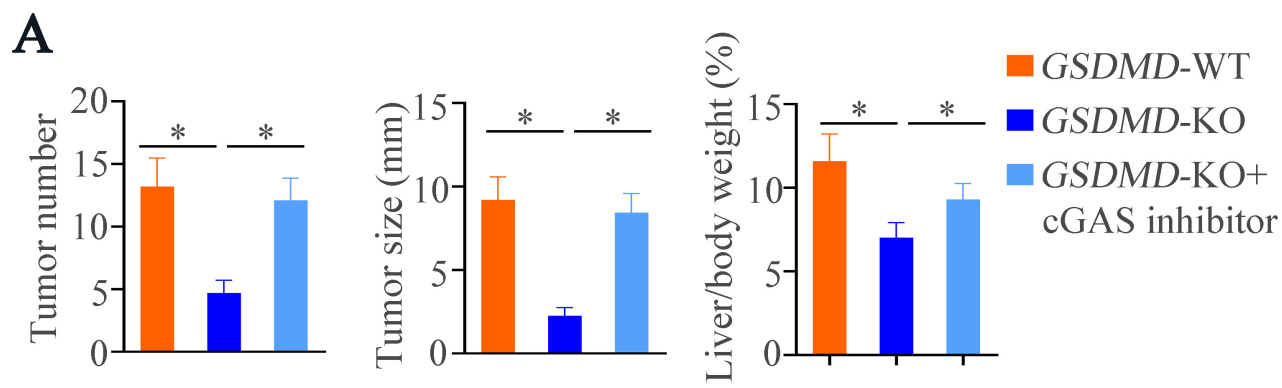
A
Tumor number
Tumor size (mm)
Liver/body weight (%)
GSDMD-WT
GSDMD-KO
GSDMD-KO+ cGAS inhibitor
B
Serum ALT (U/L)
Serum AST (U/L)
GSDMD-WT
GSDMD-KO
GSDMD-KO+ cGAS inhibitor

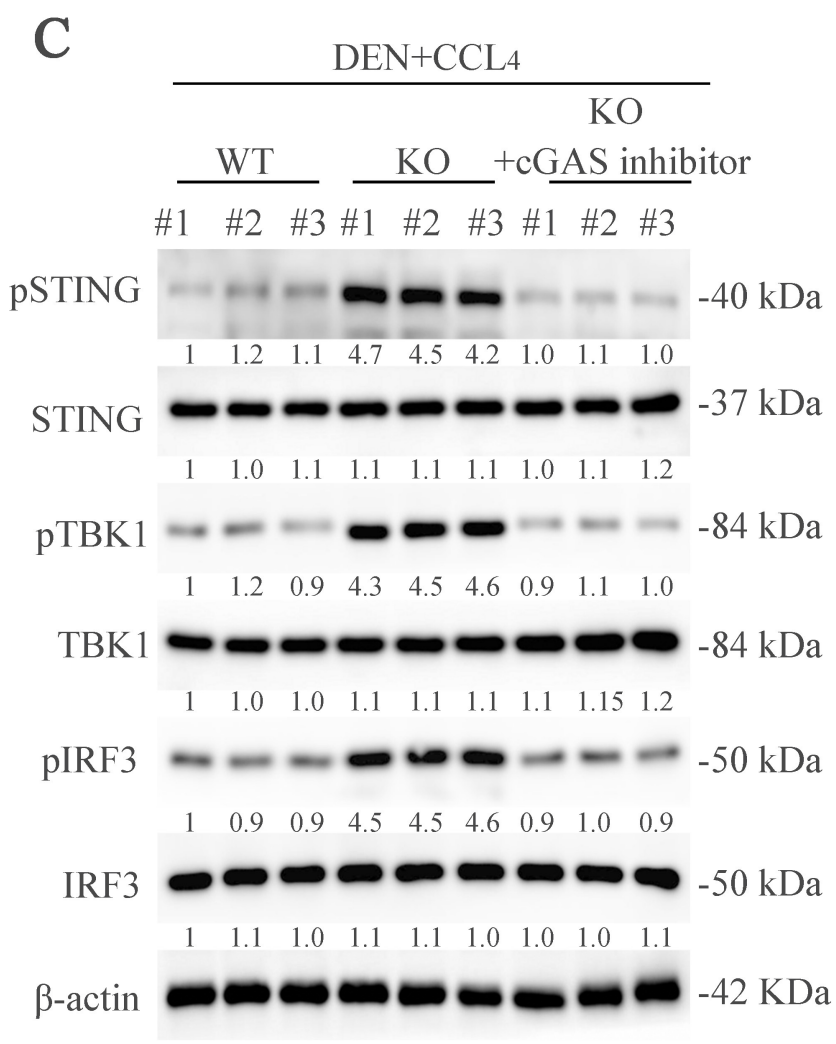
C
DEN+CCL4
WT
KO
KO +cGAS inhibitor
#1 #2 #3 #1 #2 #3 #1 #2 #3
pSTING
-40 kDa
1 1.2 1.1 4.7 4.5 4.2 1.0 1.1 1.0
STING
-37 kDa
1 1.0 1.1 1.1 1.1 1.1 1.0 1.1 1.2
pTBK1
-84 kDa
1 1.2 0.9 4.3 4.5 4.6 0.9 1.1 1.0
TBK1
-84 kDa
1 1.0 1.0 1.1 1.1 1.1 1.1 1.15 1.2
pIRF3
-50 kDa
1 0.9 0.9 4.5 4.5 4.6 0.9 1.0 0.9
IRF3
-50 kDa
1 1.1 1.0 1.1 1.1 1.0 1.0 1.0 1.1
β-actin
-42 KDa

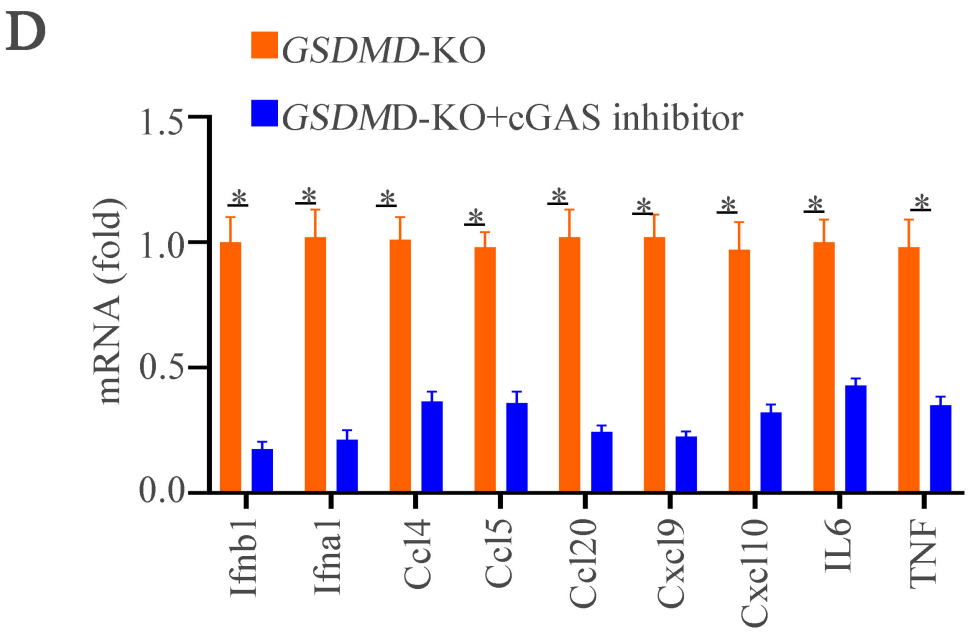
D
GSDMD-KO
GSDMD-KO+cGAS inhibitor
mRNA (fold)
Ifnb1
Ifna1
Ccl4
Ccl5
Ccl20
Cxcl9
Cxcl10
IL6
TNF

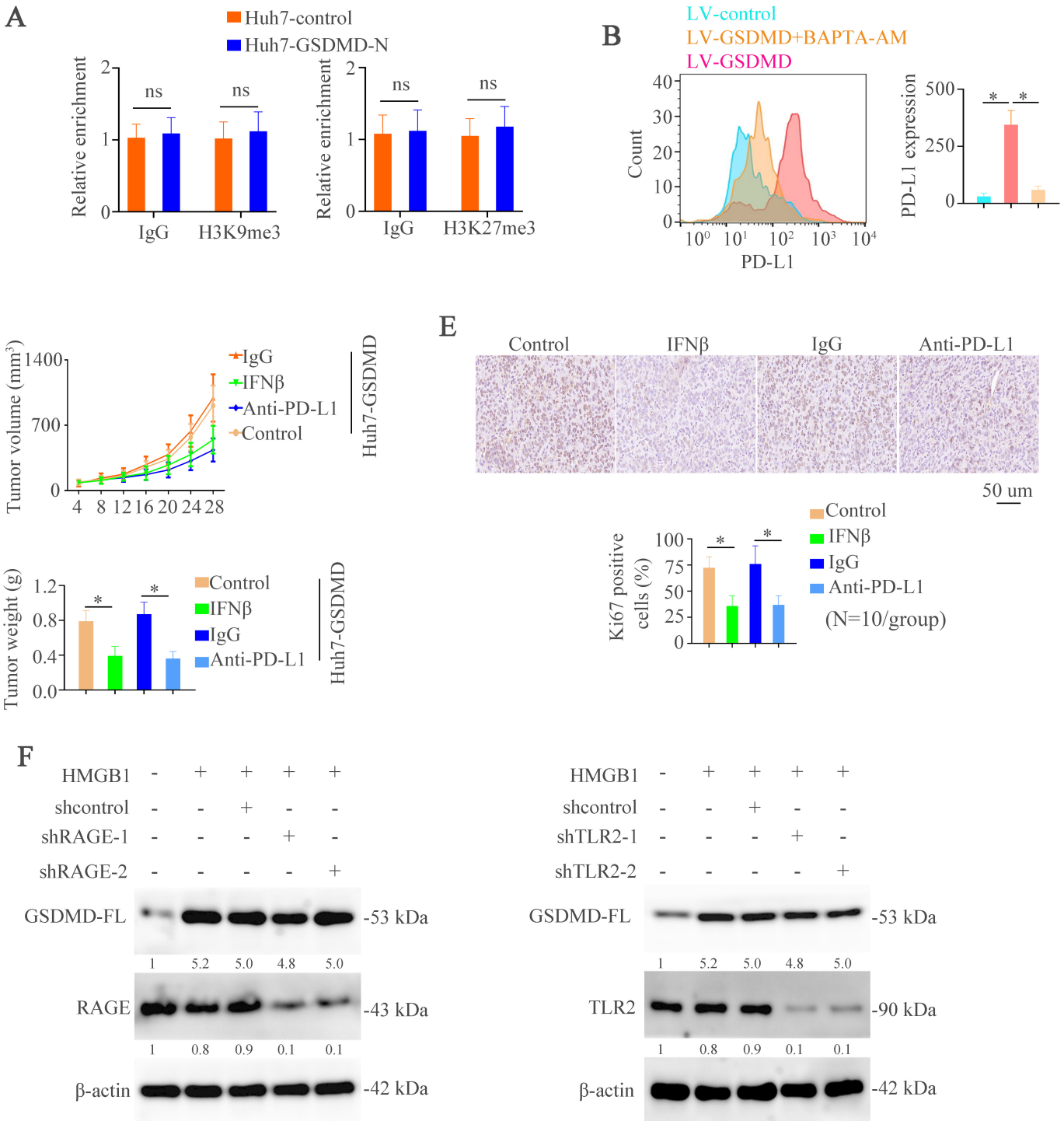
A
Huh7-control
Huh7-GSDMD-N
Relative enrichment
ns
IgG
H3K9me3
H3K27me3
B
LV-control
LV-GSDMD+BAPTA-AM
LV-GSDMD
Count
PD-L1
PD-L1 expression
C
Tumor volume (mm3)
IgG
IFNβ
Anti-PD-L1
Control
Huh7-GSDMD
D
Tumor weight (g)
E
Control
IFNβ
IgG
Anti-PD-L1
50 um
Ki67 positive cells (%)
(N=10/group)
F
HMGB1
shcontrol
shRAGE-1
shRAGE-2
shTLR2-1
shTLR2-2
GSDMD-FL
-53 kDa
RAGE
-43 kDa
TLR2
-90 kDa
β-actin
-42 kDa

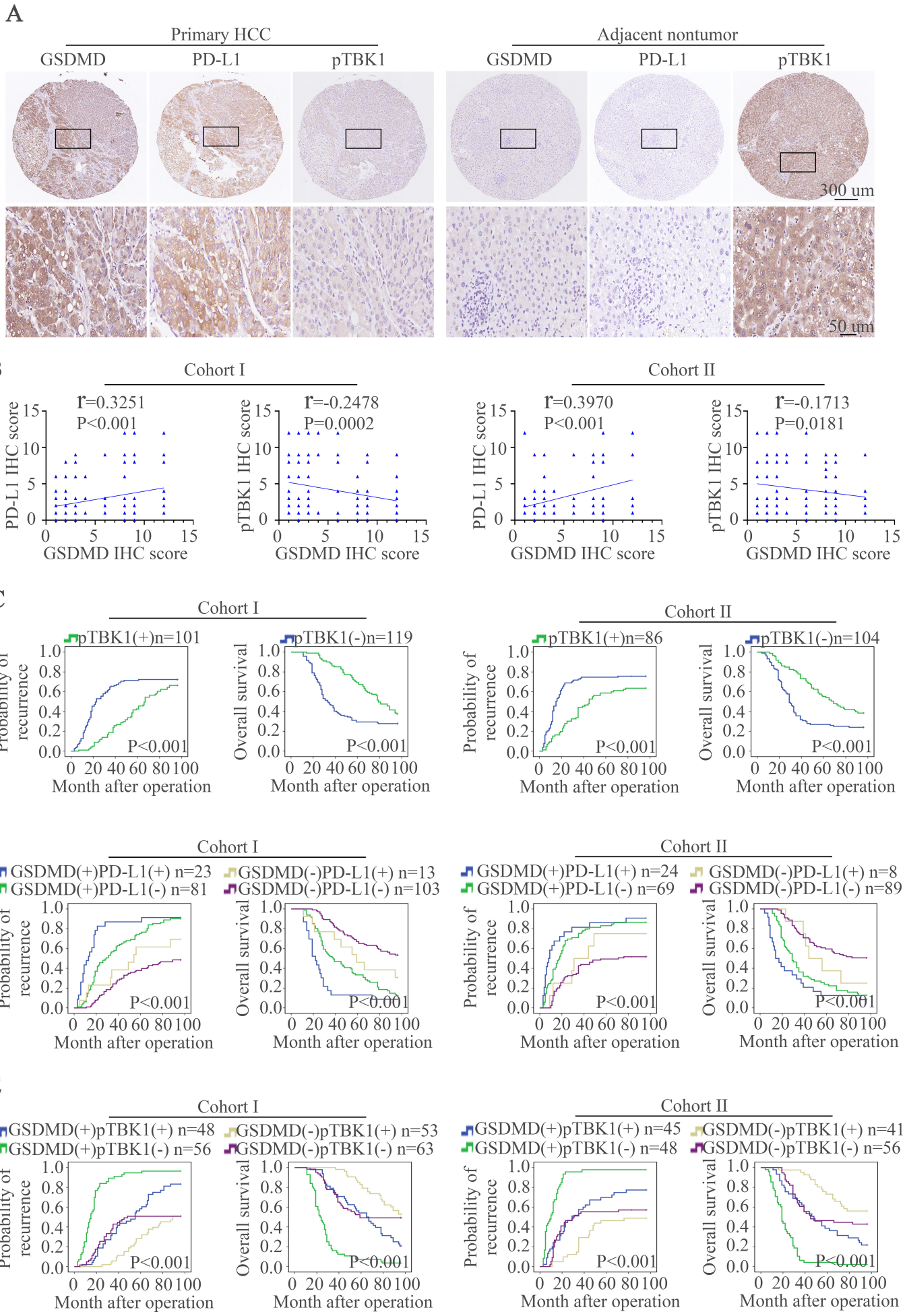
A
Primary HCC
GSDMD
PD-L1
pTBK1
Adjacent nontumor
GSDMD
PD-L1
pTBK1
300 um
50 um
B
Cohort I
r=0.3251
P<0.001
PD-L1 IHC score
GSDMD IHC score
r=-0.2478
P=0.0002
pTBK1 IHC score
GSDMD IHC score
Cohort II
r=0.3970
P<0.001
PD-L1 IHC score
GSDMD IHC score
r=-0.1713
P=0.0181
pTBK1 IHC score
GSDMD IHC score
C
Cohort I
pTBK1(+)n=101
Probability of recurrence
P<0.001
Month after operation
pTBK1(-)n=119
Overall survival
P<0.001
Month after operation
Cohort II
pTBK1(+)n=86
Probability of recurrence
P<0.001
Month after operation
pTBK1(-)n=104
Overall survival
P<0.001
Month after operation
D
Cohort I
GSDMD(+)PD-L1(+) n=23
GSDMD(+)PD-L1(-) n=81
GSDMD(-)PD-L1(+) n=13
GSDMD(-)PD-L1(-) n=103
Probability of recurrence
P<0.001
Month after operation
Overall survival
P<0.001
Month after operation
Cohort II
GSDMD(+)PD-L1(+) n=24
GSDMD(+)PD-L1(-) n=69
GSDMD(-)PD-L1(+) n=8
GSDMD(-)PD-L1(-) n=89
Probability of recurrence
P<0.001
Month after operation
Overall survival
P<0.001
Month after operation
E
Cohort I
GSDMD(+)pTBK1(+) n=48
GSDMD(+)pTBK1(-) n=56
GSDMD(-)pTBK1(+) n=53
GSDMD(-)pTBK1(-) n=63
Probability of recurrence
P<0.001
Month after operation
Overall survival
P<0.001
Month after operation
Cohort II
GSDMD(+)pTBK1(+) n=45
GSDMD(+)pTBK1(-) n=48
GSDMD(-)pTBK1(+) n=41
GSDMD(-)pTBK1(-) n=56
Probability of recurrence
P<0.001
Month after operation
Overall survival
P<0.001
Month after operation

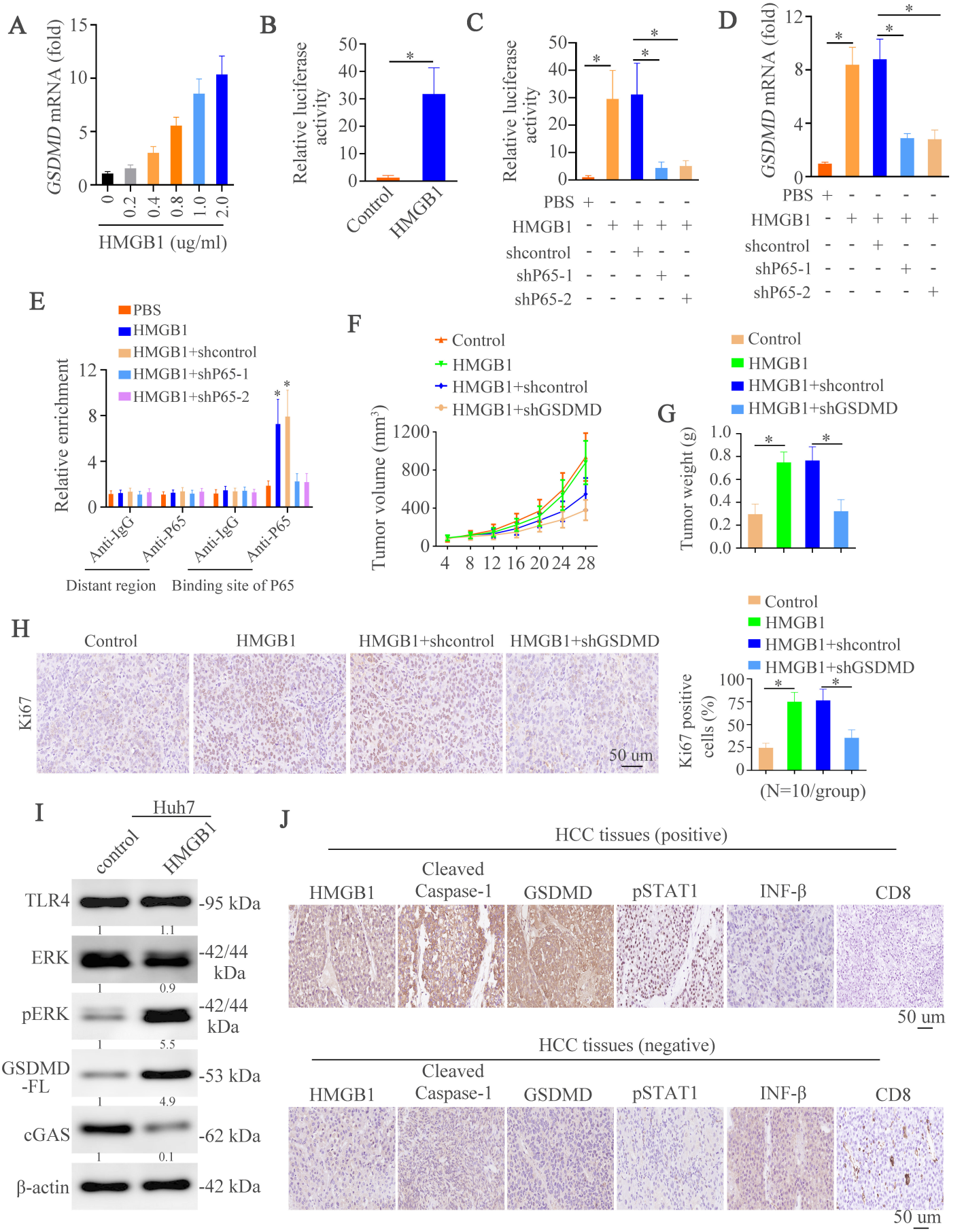
A
GSDMD mRNA (fold)
HMGB1 (ug/ml)
B
Relative luciferase activity
Control
HMGB1
C
Relative luciferase activity
PBS
HMGB1
shcontrol
shP65-1
shP65-2
D
GSDMD mRNA (fold)
E
PBS
HMGB1
HMGB1+shcontrol
HMGB1+shP65-1
HMGB1+shP65-2
Relative enrichment
Anti-IgG
Anti-P65
Distant region
Binding site of P65
F
Control
HMGB1
HMGB1+shcontrol
HMGB1+shGSDMD
Tumor volume (mm3)
G
Tumor weight (g)
H
Control
HMGB1
HMGB1+shcontrol
HMGB1+shGSDMD
Ki67
50 um
Ki67 positive cells (%)
(N=10/group)
I
Huh7
control
HMGB1
TLR4
-95 kDa
ERK
-42/44 kDa
pERK
-42/44 kDa
GSDMD -FL
-53 kDa
cGAS
-62 kDa
β-actin
-42 kDa
J
HCC tissues (positive)
HMGB1
Cleaved Caspase-1
GSDMD
pSTAT1
INF-β
CD8
50 um
HCC tissues (negative)
HMGB1
Cleaved Caspase-1
GSDMD
pSTAT1
INF-β
CD8
50 um

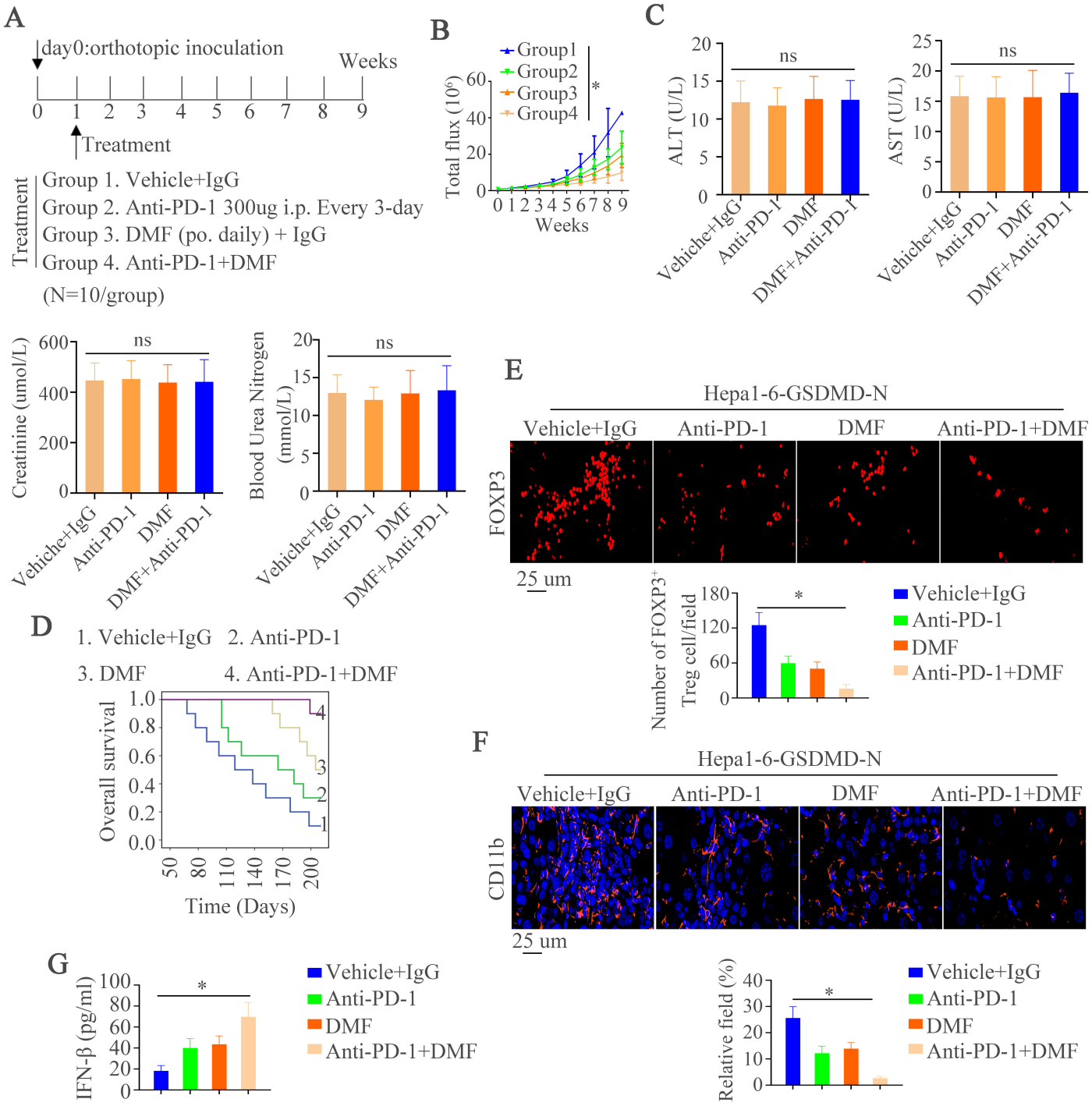
A
day0:orthotopic inoculation
Weeks
0 1 2 3 4 5 6 7 8 9
Treatment
Treatment
Group 1. Vehicle+IgG
Group 2. Anti-PD-1 300ug i.p. Every 3-day
Group 3. DMF (po. daily) + IgG
Group 4. Anti-PD-1+DMF
(N=10/group)
B
Group1
Group2
Group3
Group4
*
Total flux (10^6)
Weeks
C
ns
ALT (U/L)
AST (U/L)
Vehiche+IgG
Anti-PD-1
DMF
DMF+Anti-PD-1
Creatinine (umol/L)
Blood Urea Nitrogen (mmol/L)
D
1. Vehicle+IgG 2. Anti-PD-1
3. DMF 4. Anti-PD-1+DMF
Overall survival
Time (Days)
E
Hepa1-6-GSDMD-N
Vehicle+IgG
Anti-PD-1
DMF
Anti-PD-1+DMF
FOXP3
25 um
Number of FOXP3+ Treg cell/field
F
CD11b
Relative field (%)
G
IFN-β (pg/ml)

Supplementary material

Methods

Cell culture

Immortalized liver cell line (HL-7702) was purchased from the Institute of Biochemistry and Cell Biology, Chinese Academy of Science, China. Human HCC cells (HepG2, Huh-7, Hep3B, PLC/PRF/5) were purchased from the American Type Culture Collection. Additional human HCC cells (MHCC97H, HCCLM3, and HCCLM6) were kindly provided by Dr. Tang ZY (Liver Cancer Institute, Zhongshan Hospital, Fudan University, Shanghai, China). Cells were cultured in Dulbecco's Modified Eagle Medium (DMEM) 37°C in a 5% CO2 incubator. The medium was supplemented with 10% FBS, 100μg/ml penicillin, and 100μg/ml streptomycin. These above cell lines were authenticated by short tandem repeats (STRs) DNA profiling. All cells were tested for mycoplasma contamination before use with the Universal Mycoplasma Detection Kit (ATCC 30-1012K) and were not contaminated by mycoplasma.

Construction of plasmid, lentivirus and stable cell lines

Plasmid and lentivirus construction were performed by DesignGene Biotechnology (Shanghai China) according to standard procedures. The constructs were confirmed by DNA sequencing. The lentivirus transfection was performed according to stand procedure as previous described (1). Briefly, lentivirus was added to the target cells in cell culture media with 5 μg/ml polybrene (Sigma H9268). Twenty-four hours later, the media was replaced by DMEM with 10% FBS. Seventy-two hours after infection, cells

were selected for 2 weeks using 2.5 μg/ml puromycin (OriGene). Selected pools of cells were used for the following experiments.

Transient transfection

The cells were plated at a density of 1×10^5 cells/well in a 24-well plate. After 12-24 hours, the cells were co-transfected with 0.6μg of expression vector plasmids, 0.18μg of promoter reporter plasmids, and 0.02μg of pRL-TK plasmids using Lipofectamine 3000 (Invitrogen, USA) according to the manufacturer's instructions. After 6h of transfection, the cells were washed and allowed to recover overnight in fresh medium supplemented with 1% FBS for 48 h. Serum-starved cells were used for the assay.

Luciferase reporter assay

Luciferase activity was detected using the Dual Luciferase Assay (Promega, USA) according to the manufacturer's instructions. The transfected cells were lysed in culture dishes containing a lysis buffer and the resulting lysates were centrifuged at maximum speed for 1 min in a microcentrifuge. Relative luciferase activity was determined using a ModulusTM TD20/20 Luminometer (Turner Biosystems, USA), and the transfection efficiencies were normalized according to the Renilla activity.

Western blot analysis

Proteins from lysed cells were fractionated by SDS-PAGE and transferred to nitrocellulose membranes. Nonspecific binding sites were blocked with 5% BSA in TBST for 2 hours at room temperature. Blots were incubated with a specific antibody overnight at 4 °C. The membranes were then washed with TBST 3 times and incubated with an HRP-conjugated secondary antibody. Proteins were visualized using an

ImmobilonTM Western Chemiluminescent HRP substrate (Millipore, USA).

The primary antibodies used are listed below.

Antibodies	Source
anti-GSDMD	Abcam, ab210070
anti-GSDMD-N	Abcam, ab215203
anti-pSTING	Cell signaling technology, #50907
anti-STING	Cell Signaling Technology, #13647
anti-pTBK1	Abcam, ab109272
anti-TBK1	Abcam, ab40676
anti-pIRF3	Abcam, ab76493
anti-IRF3	Abcam, ab68481
anti-PD-L1	Cell signaling technology, #13684
anti-STAT1	Abcam, ab92506
anti-pSTAT1	Abcam, ab29045
anti-Calmodulin	Abcam, ab45689
anti-HDAC1	Cell signaling technology, #34589
anti-pP65	Cell signaling technology, #3033
anti-P65	Cell signaling technology, #8242
anti-TLR4	Abcam, ab13556
anti-RAGE	Abcam, ab216329
anti-TLR2	Abcam, ab213676
anti-Caspase-1	Cell signaling technology, #3866

anti-p-ERK1/2(T202/Y204)	Cell Signaling Technology, #4370
anti-ERK	Cell Signaling Technology, #4695
anti-JNK	Abcam, ab179461
anti-JNK (phosphoT183+T183+T221))	Abcam, ab124956
anti-p38	Cell Signaling Technology, #8690
anti-p-p38(Thr180/Tyr182)	Cell Signaling Technology, #4511
anti-AKT	Cell signaling technology, #4685
anti-p-AKT(Ser-473)	Cell signaling technology, #4060
anti-β-actin	Proteintech, 60008-1-Ig

Quantitative Real-time PCR (RT-qPCR)

The RNeasy Plus Mini Kit (50) kit (Qiagen, Hilden, Germany) was used to extract total RNA, which was then reverse transcribed with the Advantage RT-for-PCR Kit (Qiagen) in accordance with the manufacturer's protocols. The target sequence was amplified with RT-qPCR with the SYBR Green PCR Kit (Qiagen). The cycling parameters used were 95 °C for 15 s, 55-60 °C for 15 s, and 72 °C for 15 s for 45 cycles. The $2^{-\Delta\Delta Ct}$ method was used to determine relative fold changes in target gene expression. All experiments were performed in triplicate. The primer sequences were listed in Supplementary Table S4.

Chromatin immunoprecipitation Assay (ChIP)

Chromatin immunoprecipitation assays were conducted with a Magana CHIP A/G (catalog #17-10085, Merck Millipore). In briefly, 1% formaldehyde was used to crosslink the treated cells at 37 °C for 10 min and then the cells were resuspended in

300 μl of lysis buffer. The DNA was sheared to small fragments by sonication. The fragment DNA were incubated with specific antibodies or isotype control IgG. Then, RT-qPCR was used to amplify the corresponding binding site on the promoters. The $2^{-\Delta\Delta Ct}$ method was used to determine relative fold changes in target gene expression in cell lines, which was normalized to expression levels in corresponding control cells (defined as 1.0). The primers were shown in Supplementary Table S4.

For ChIP assays of tissues, cells were first separated from six pairs of fresh frozen HCC tissues and normal liver tissues collected after surgical resection. Tissue was cut into small piece (typical $1mm^3$ or smaller). Then, digestion the tissues with DNase I (20 mg/mL; Sigma-Aldrich) and collagenase (1.5 mg/mL; Sigma-Aldrich) for 1h at 37℃. Then, the cells were dissociated through 70μm-pore filters rinsed with fresh media followed by red cell lysis. The dissociated cells were crosslinked using 1% formaldehyde for 10 minutes at 37℃. After cell lysis, the DNA was fragmented by sonication. ChIP grade antibody or IgG (negative control) was used to immunoprecipitated the fragment DNA. Then, RT-qPCR was used to amplify the corresponding binding site on the promoters.

Construction of tissue microarrays and immunohistochemistry

HCC samples and the corresponding adjacent liver tissues were used to construct a tissue microarray (Shanghai Biochip Co., Ltd. Shanghai, China). IHC was performed on 4-μm-thick, routinely processed paraffin-embedded sections. Briefly, the tissue sections were deparaffinized after baking at 60 °C for an hour. Endogenous peroxidase activity was blocked by 3% (vol/vol) hydrogen peroxide in methanol for 12 min and

washes with PBS. Then the slides were immersed in 0.01 mol/L citrate buffer solution or EDTA for 30 min using a microwave. Primary antibody was added in the tissues in 4 °C for overnight. The tissue microarrays were stained for GSDMD (Proteintech, 20770-1-AP), PCNA (cell signaling technology, # 13110), γH2AX (cell signaling technology, # 9718), PD-L1 (cell signaling technology, #13684) and pIRF3 (Abbexa, abx012441)). The sections were treated with a peroxidase-conjugated second antibody (Santa Cruz) for 30 min at room temperature and then washed with PBS. Reaction product was visualized with diaminobenzidine for 2 min. Images were obtained under a light microscope (Olympus, Japan) equipped with a DP70 digital camera. Analyses were performed by two independent observers who were blinded to the clinical outcome. The immunostaining intensity score was described as previous work (1) and briefly described as following. Analyses were performed by two independent observers who were blinded to the clinical outcome. The immunostaining intensity was scored on a scale of 0 to 3: 0 (negative), 1 (weak), 2 (medium) or 3 (strong). The percentage of positive cells was evaluated on a scale of 0 to 4: 0 (negative), 1 (1%-25%), 2 (26%-50%), 3 (51%-75%), or 4 (76%-100%). The final immuno-activity scores were calculated by multiplying the above two scores, resulting an overall score which range from 0~12. Each case was ultimately considered “negative” if the final score ranges from 0~3, and “positive” if the final score ranges from 4~12.

Immunofluorescence (IF)

Formalin-fixed paraffin-embedded sections (4μm) were baked, deparaffinized, rehydrated, followed by antigen retrieval and permeabilized. After that the tissues were

blocked with 10% goat or donkey serum for 30 minutes and incubated with primary antibodies at 4°C overnight. After washing, appropriate secondary antibodies were used. The DAPI was used to stain cell nucleus for ten minutes. Florescence was visualized under an Olympus fluorescence microscope.

Antibodies used in Immunofluorescence

Antibodies	Source
Anti-αSMA	Abcam, ab124964
Anti-cGAS	Cell signaling technology, #79978
Anti-Calmodulin	Abcam, ab2860
Anti-CD8a	Invitrogen, 4SM15
Anti-Granzyme B	R&D, AF1865

Preparation of Single Cell Suspensions

Primary to flow cytometry analysis, single cell suspensions should be prepared. The method was used as described in the research paper (1). Briefly, after the anesthetization of mice, Hank's buffer without calcium was first injected into the liver through the portal vein and then the Hank's buffer including calcium, magnesium and collagenase IV (0.2 mg/mL, Sigma-Aldrich, C5138) followed. After separation of the liver and tumor, the tissues were made into small pieces about $1mm^3$. Mouse tumor dissociation buffer (Miltenyi, 130-096-730) was used to prepare the single cell by using the gentleMACS dissociator (Miltenyi Biotech) followed by filtrating through a 70 μm cell mesh, lysing erythrocyte, centrifuging, and resuspending in Hank's buffer.

Flow cytometry

After the anesthetization of mice, tumors were collected to prepare the single cell suspensions according to the procedure described above. Fc block was added to the cells at room temperature for 10 minutes and then incubated with primary antibodies or isotype antibodies at 4°C for 45 minutes. A FACS LSRFortessa and FlowJo software (BD Biosciences) were used to acquire and analyze the data respectively.

Antibodies used in Flow Cytometric Analysis

Antibodies	Source
anti-CD45	BD, 559864
anti-CD3	BD, 555275
anti-CD8a	BD, 564459
7-AAD	Absin, abs9104

Animals and animal models

The C57BL/6J wild-type (WT) mice, GSDMD-/- mice, and Alb-Cre mice were purchased from the Cyagen Biosciences. 11 exons of *GSDMD* gene are identified , with the ATG start codon in exon 2 and the TAG stop codon in exon 11. Exon 2~11 were selected as target site. Cas9 and gRNA will be co-injected into fertilized eggs for KO mouse production.

Detection of orthotopic inoculation mouse tumor in vivo

For in vivo signal detection, D-luciferin (Perkin-Elmer) at 100 mg/kg was injected intraperitoneally into the mice, and bioluminescence was detected using a Lago X optical imaging system (SI Imaging). At the end point, the mice were sacrificed, and their livers and lungs were dissected and prepared for standard histological examination. This message was introduced in the supplementary material

Transmission electron microscope (TEM)

The liver tissues and HCC cells were prefixed with a 3% glutaraldehyde, and was postfixed in 1% osmium tetroxide, dehydrated in series acetone, infiltrated in Epox 812 for a longer, and embeded. The semithin sections were stained with methylene blue and Ultrathin sections were cut with diamond knife, stained with uranyl acetate and lead citrate. Sections were examined with JEM-1400-FLASH Transmission Electron Microscope.

References

1. He Q, Liu M, Huang W, Chen X, Zhang B, Zhang T, Wang Y, et al. IL-1beta-Induced Elevation of Solute Carrier Family 7 Member 11 Promotes Hepatocellular Carcinoma Metastasis Through Up-regulating Programmed Death Ligand 1 and Colony-Stimulating Factor 1. Hepatology 2021;74:3174-3193.

Supplementary Table S1. Correlation between GSDMD expression and clinicopathological characteristics of HCCs in two independent cohorts of human HCC tissues

		Cohort I			Cohort II		
		Tumor GSDMD expression			Tumor GSDMD expression		
		Negative	Positive	*P*	Negative	Positive	*P*
Clinicopathological variables		(n=116)	(n=104)	Value	(n=97)	(n=93)	Value
Age		52.95(11.500)	50.73(13.027)	0.149	51.38(7.943)	50.44(8.320)	0.562
Sex	female	21	19	1.000	14	17	0.557
	male	95	85		83	76	
Serum AFP	≤20ng/ml	23	26	0.418	21	22	0.863
	>20ng/ml	93	78		76	71	
Virus infection	HBV	88	70	0.476	70	71	0.752
	HCV	10	15		9	10	
	HBV+HCV	5	6		5	3	
	none	13	13		13	9	
Cirrrhosis	absent	33	26	0.648	21	21	1.000
	present	83	78		76	72	
Child-pugh score	Class A	84	81	0.436	84	74	0.245
	Class B	32	23		13	19	
Tumor number	single	76	45	0.001	66	48	0.026
	multiple	40	59		31	45	
Maximal tumor size	≤5cm	49	34	0.165	68	39	<0.001
	>5cm	67	70		29	54	
Tumor encapsulation	absent	35	64	<0.001	17	48	<0.001
	present	81	40		80	45	
Microvascular invasion	absent	84	37	0.001	77	26	<0.001
	present	32	67		20	67	
Tumor differentiation	I-II	101	70	0.001	86	47	<0.001
	III-Ⅳ	15	34		11	46	
TNM stage	I-II	104	50	<0.001	88	49	<0.001
	III	12	54		9	44	

Supplementary Table 2. Univariate and multivariate analysis of factors associated with survival and recurrence in two independent cohorts of human HCC

	Time To Recurrence		Overall Survival	
Clinical Variables	HR(95% CI)	P value	HR(95% CI)	P value
Univariate analysis				
Cohort I(n=220)				
Age (≤50 versus > 50)	0.988(0.976-1.001)	0.077	0.987(0.974-1.000)	0.053
Sex (female versus male)	1.224(0.817-1.834)	0.327	1.261(0.840-1.892)	0.263
Serum AFP (≤20 versus >20 ng/ml)	0.705(0.472-1.051)	0.086	0.680(0.451-1.026)	0.066
HBV infection (no versus yes)	0.615(0.267-1.416)	0.254	0.655(0.284-1.506)	0.319
Cirrhosis (absent versus present)	1.054(0.739-1.504)	0.771	1.038(0.725-1.488)	0.838
Child-pugh score (A versus B)	1.201(0.826-1.745)	0.337	1.259(0.859-1.847)	0.238
Tumor number (single versus multiple)	0.491(0.357-0.675)	<0.001	0.460(0.333-0.637)	<0.001
Maximal tumor size (≤5cm versus >5)	0.661(0.472-0.925)	0.016	0.654(0.463-0.922)	0.015
tumor encapsulation (present versus absent)	2.627(1.902-3.626)	<0.001	2.728(1.966-3.784)	<0.001
Microvascular invasion (absent versus present)	0.386(0.279-0.533)	<0.001	0.367(0.264-0.509)	<0.001
Tumor differentiation (I-II versus III-IV)	0.513(0.356-0.740)	<0.001	0.481(0.333-0.695)	<0.001
TNM stage (I-II versus III)	0.089(0.060-0.132)	<0.001	0.082(0.055-0.123)	<0.001
GSDMD expression (negative versus positive)	0.302(0.217-0.420)	<0.001	0.307(0.220-0.429)	<0.001
Multivariate analysis				
Tumor number (single versus multiple)	0.857(0.536-1.371)	0.520	0.787(0.493-1.258)	0.317
Maximal tumor size (≤5cm versus >5)	0.729(0.498-1.069)	0.106	0.744(0.503-1.099)	0.137
Tumor encapsulation (present versus absent)	1.460(0.935-2.279)	0.096	1.356(0.865-2.125)	0.185
Microvascular invasion (absent versus present)	0.669(0.430-1.041)	0.075	0.584(0.376-0.907)	0.017
Tumor differentiation (I-II versus III-IV)	1.351(0.887-2.056)	0.161	1.237 (0.815-1.878)	0.317
TNM stage (I-II versus III)	0.137(0.080-0.232)	<0.001	0.130(0.076-0.223)	<0.001
GSDMD expression (negative versus positive)	0.576(0.399-0.833)	0.003	0.607(0.420-0.877)	0.008
Cohort II(n=190)				
Age (≤50 versus > 50)	1.002(0.981-1.023)	0.859	0.998(0.977-1.019)	0.854

Sex (female versus male)	1.317(0.851-2.039)	0.217	1.250(0.802-1.949)	0.324
Serum AFP (≤20 versus >20 ng/ml)	1.096(0.738-1.626)	0.650	1.143(0.770-1.696)	0.508
HBV infection (no versus yes)	1.170(0.425-3.222)	0.761	0.995(0.361-2.739)	0.992
Cirrhosis (absent versus present)	1.029(0.684-1.547)	0.891	1.080(0.721-1.617)	0.710
Child-pugh score (A versus B)	0.705(0.459-1.083)	0.111	0.683(0.444-1.050)	0.083
Tumor number (single versus multiple)	0.442(0.313-0.625)	<0.001	0.442(0.313-0.625)	<0.001
Maximal tumor size (≤5cm versus >5)	0.544(0.386-0.766)	<0.001	0.550(0.390-0.776)	0.001
Tumor encapsulation (present versus absent)	1.987(1.401-2.819)	<0.001	1.982(1.397-2.811)	<0.001
Microvascular invasion (absent versus present)	0.387(0.273-0.548)	<0.001	0.389(0.274-0.552)	<0.001
Tumor differentiation (I-II versus III-IV)	0.229(0.159-0.330)	<0.001	0.251(0.175-0.360)	<0.001
TNM stage (I-II versus III)	0.141(0.094-0.211)	<0.001	0.136(0.091-0.203)	<0.001
GSDMD expression (negative versus positive)	0.343(0.241-0.489)	<0.001	0.315(0.220-0.450)	<0.001
Multivariate analysis				
Tumor number (single versus multiple)	0.813(0.527-1.252)	0.346	0.838(0.545-1.288)	0.419
Maximal tumor size (≤5cm versus >5)	1.036(0.689-1.557)	0.866	1.055(0.700-1.589)	0.870
Tumor encapsulation (present versus absent)	0.953(0.625-1.453)	0.822	0.985(0.649-1.495)	0.945
Microvascular invasion (absent versus present)	0.868(0.534-1.411)	0.567	1.021(0.624-1.670)	0.934
Tumor differentiation (I-II versus III-IV)	0.606(0.362-1.016)	0.058	0.781(0.460-1.326)	0.359
TNM stage (I-II versus III)	0.288(0.152-0.545)	<0.001	0.232(0.121-0.446)	<0.001
GSDMD expression (negative versus positive)	0.588(0.376-0.919)	0.020	0.468(0.298-0.732)	0.001

Supplementary Table S3. Correlation between pTBK1 expression and clinicopathological characteristics of HCCs in two independent cohorts of human HCC tissues

		Cohort I			Cohort II		
		Tumor pTBK1 expression			Tumor pTBK1 expression		
Clinicopathological variables		Negative (n=119)	Positive (n=101)	*P* Value	Negative (n=104)	Positive (n=86)	*P* Value
Age		51.84(12.530)	51.97(12.014)	0.529	51.45(7.537)	50.28(8.779)	0.161
Sex	female	24	16	0.484	17	14	1.000
	male	95	85		87	72	
Serum AFP	≤20ng/ml	18	31	0.009	22	21	0.606
	>20ng/ml	101	70		82	65	
Virus infection	HBV	85	73	0.590	72	69	0.296
	HCV	12	13		13	6	
	HBV+HCV	8	3		6	2	
	none	14	12		13	9	
Cirrrhosis	absent	32	27	1.000	23	19	1.000
	present	87	74		81	67	
Child-pugh score	Class A	90	75	0.876	85	73	0.697
	Class B	29	26		19	13	
Tumor number	single	63	58	0.587	52	62	0.003
	multiple	56	43		52	24	
Maximal tumor size	≤5cm	36	47	0.017	54	53	0.189
	>5cm	83	54		50	33	
Tumor encapsulation	absent	62	37	0.029	43	22	0.031
	present	57	64		61	64	
Microvascular invasion	absent	61	60	0.227	51	52	0.144
	present	58	41		53	34	
Tumor differentiation	I-II	83	88	0.002	63	70	0.002
	III-Ⅳ	36	13		41	16	
TNM stage	I-II	65	89	<0.001*	62	75	<0.001*
	III	54	12		42	11	

Supplementary Table S4. Primer sequences used in the study

Primer name	Primer sequences	Enzyme
Primers for real-time PCR:		
GSDMD sense:	5'-GTGTGTCAACCTGTCTATCAAGG-3'	
GSDMD antisense:	5'-CATGGCATCGTAGAAGTGGAAG-3'	
IFNb1 sense:	5'- ATGACCAACAAGTGTCTCCTCC -3'	
IFNb1 antisense:	5'- GGAATCCAAGCAAGTTGTAGCTC -3'	
IFNa1 sense:	5'-GCCTGTGCTATGGCGAGTTT-3'	
IFNa1 antisense:	5'- GCCTCGCCCTTTGCTTTACT-3'	
IFNa1 sense:	5'- CTGTGGGTCTCAGGGAGATCA -3'	
IRF3 antisense:	5'- CTACGGCAGGACGCACAGAT -3'	
IRF3 sense:	5'- TCAGCAGCTAACCGCAACAC-3'	
IRF7 antisense:	5'- CAGCACAGGGCGTTTTATCTT-3'	
IRF7 sense:	5'- TCTTCCCTATTTTCCGTGGC-3'	
IFIT1 antisense:	5'- TGCTTTGCGAAGGCTCTGA -3'	
IFIT1 sense:	5'- AATCTTGGCGATAGGCTACGAC-3'	
Ccl4 antisense:	5'- GCTCTGTGCAAACCTAACCC -3'	
Ccl4 sense:	5'- GAAACAGCAGGAAGTGGGAG -3'	
Ccl5 antisense:	5'- GACACCACTCCCTGCTGCTT-3'	
Ccl5 sense:	5'- ACACTTGGCGGTTCCTTCG-3'	
Ccl20 antisense:	5'- TGTACGAGAGGCAACAGTCG-3'	
Ccl20 sense:	5'- TCTGCTCTTCCTTGCTTTGG-3'	
Cxcl9 antisense:	5'- CCAGTAGTGAGAAAGGGTCGC-3'	
Cxcl9 sense:	5'- AGGGCTTGGGGCAAATTGTT-3'	
Cxcl10 antisense:	5'- AAGTGCTGCCGTCATTTTCTG-3'	
Cxcl10 sense:	5'- TTCCCTATGGCCCTCATTCTC-3'	
Ddx41 antisense:	5'- AGTCCGCCAAGGAAAAGCAA-3'	
Ddx41 sense:	5'- CTCAGACATGCTCAGGACATAAC-3'	
IL6 antisense:	5'-CTTGGGACTGATGCTGGTGAC-3'	
IL6 sense:	5'-CTGCCTACACCTACAGCTATGT-3'	
Polr1c sense:	5'- CGCAATGTCCATACTACTGACTT-3'	
Polr1c antisense:	5'- CCACACGGAAATTCTTCTCGAA-3'	
Polr2e sense:	5'- GGTGGGCATCAAGACCATCAA-3'	
Polr2e antisense:	5'- TCAGGGACTAGCTCGTGCTC-3'	
TNF sense:	5'- TACTGAACTTCGGGGTGATCG-3'	
TNF antisense:	5'- TCCTCCACTTGGTGGTTTGC-3'	
ACTB sense:	5'-CATGTACGTTGCTATCCAGGC-3'	
ACTB antisense:	5'-CTCCTTAATGTCACGCACGAT-3'	
Primers for *CD274* promoter construct:		
(-1970/+214) *CD274* sense:	5'-TATAGGTACCCAATCTCCGGGTAGTTGA-3'	kpnl
(-1230/+214) *CD274* sense:	5'-TATAGGTACCAAGGAACATCTGAGCTGG-3'	
(-715/+214) *CD274* sense:	5'- TATAAGATCTGCAGCCTTAATCCTTAGG-3'	
(-258/+214) *CD274* sense:	5'- TATAAGATCTGAAACTCTTCCCGGTGAA-3'	
(-110/+214) *CD274* sense:	5'- TATAAGATCTAGTATCTCTGGCTAGCTC-3'	

Antisense:	5’- ATATAAGCTTGGTAATTGGCTCTACTGC-3’	nhel
Primers for *CD274* promoter site-directed mutagenesis:		
Stat1 binding site:		
mutation sense:	5’-AAATCTCATTTAtcctAAAACTGGACT-3’	
mutation antisense:	5’-AGTCCAGTTTTaggaTAAATGAGATTT-3’	
HIF1α binding site:		
mutation sense:	5’-TGAGCAGCaataTCCCGCGCGGC-3’	
mutation antisense:	5’-GCCGCGCGGGAtattGCTGCTCA-3’	
Primers for *GSDMD* promoter construct:		
(-1989/+132) GSDMD sense:	5’-TATAGGTACCTCACTATCTGATTGTCAA-3’	KpnI
(-1486/+132) GSDMD sense:	5’-TATACTCGAGGATCTTGGCTCACTGCAA-3’	KpnI
(-957/+132) GSDMD sense:	5’-TATACTCGAGCAGGGAGCAACACTCCTT-3’	KpnI
(-521/+132) GSDMD sense:	5’-TATACTCGAGTGAAGCTGTGAAGAGGCA-3’	KpnI
(-107/+132) GSDMD sense:	5’-TATACTCGAG TCTTGGCTCCTAGAACCA-3’	KpnI
Antisense:	5’-ATATACGCGTCCAGTTTACGGAAGTCGG-3’	MluI
Primers for *GSDMD* promoter site-directed mutagenesis:		
STAT1 binding site:		
binding site mutation sense:	5’-GAGTGAGGCTGttctGACATAGTGGGG-3’	
binding site mutation antisense:	5’-CCCCACTATGTCagaaCAGCCTCACTC-3’	
P65 binding site		
binding site mutation sense:	5’-ACATAGTGGGGgactCCCCGGCACCC-3’	
binding site mutation antisense:	5’-GGGTGCCGGGGagtcCCCCACTATGT-3’	
SP1 binding site		
binding site 1 mutation sense:	5’-CACCTGAAGTCCtattCTGCGCGGGGC-3’	
binding site 1 mutation antisense:	5’-GCCCCGCGCAGaataGGACTTCAGGTG-3’	
binding site 2 mutation sense:	5’-CTGGCTGGTCCCagaaTCCGTGCTCTG-3’	
binding site 2 mutation antisense:	5’-CAGAGCACGGAttctGGGACCAGCCAG-3’	
binding site 3 mutation sense:	5’-TCTGCGCGCCTCtcttCTAGCGCTTGT-3’	
binding site 3 mutation antisense:	5’-ACAAGCGCTAGaagaGAGGCGCGCAGA-3’	
Primers used for ChIP in the *GSDMD* promoter:		
distant region sense:	5’-GATTACAGGCATGAGCCA-3’	
distant region antisense:	5’-GCCGTCACTGCCAGGATC-3’	
P65 distant site sense:	5’-TGAGGCTGCCAGGACATA-3’	
P65 distant site antisense:	5’-TTCAGGTGCCTGCCAGAC-3’	

Supplementary Table S5 RNA-Sequencing raw data

gene_id	Expression_ NC1	Expression_ NC2	Expression_ NC3	Expression_ KO1	Expression_ KO2	Expression_ KO3
GSDMD	10.39669	10.32866	10.33395	0	0.000044551	0.000003514
POLR3C	0.073587	0.028907	0.050854	2.429528	2.593845559	2.209559702
POLR3GL	0.111462	0.065677	0.082529	4.536198	4.031395966	3.66213596
POLR1C	0.221945	0.305146	0.460136	12.69643	12.97606464	19.70905535
IRF7	0.146514	0.079689	0.151876	4.045148	4.010806462	3.585657946
RELA	0.016475	0.038831	0.042695	0.880533	0.804082704	1.2472505
IL6	1.057252	0.788838	0.788838	7.698734	5.855093975	6.919699
POLR1D	0.315709	0.47835	0.280511	9.02271	11.69384481	10.0702483
CXCL10	1.027608	1.376221	0.669443	12.66181	15.28160726	13.75883185
PYCARD	3.538454	2.957907	3.160279	0.294171	0.267659743	0.234661426
IRF3	20.13827	15.11873	18.63418	1.991023	1.506428935	1.535447065
CCL5	0.024052	0.009352	0.005876	1.134894	1.090322134	1.190678104
CCR6	9.854451	7.181346	7.682667	0.69989	0.851268768	0.894361077
IL1a	0.488811	0.683101	0.581498	6.046422	4.520457623	5.503901016
CXCL9	3.481997	3.235864	1.94072	23.03988	24.8889456	24.101197
IL1R1	1.857771	1.302949	1.348812	0.206525	0.206484656	0.151359759
IRF6	0.152692	0.132986	0.149209	1.264311	0.910110943	1.129811769
SOX9	71.14077	63.83218	61.66693	9.344868	9.57141941	8.885208901
PTAFR	20.28154	17.22706	18.3943	2.557031	2.831170076	2.792659726
CXCR4	20.28154	17.22706	18.3943	2.557031	2.831170076	2.792659726
PLCD1	3.730377	2.321773	3.348226	0.486304	0.635950243	0.286838219
SLC25A4	1.226683	0.838719	0.986672	0.198602	0.147083978	0.141394544
ISG15	17.7765	10.86745	14.28875	2.767999	2.290072532	1.945269259
CAMK2B	4.426638	2.842071	3.560527	0.880491	0.520155342	0.440206825
PHKG1	573.3711	571.0945	595.3916	107.8942	108.756529	80.52148514
TLR9	0.784416	0.847403	0.738981	5.498618	3.629422208	4.682023689
GRIN1	0.586425	0.367135	0.417922	0.119809	0.055900079	0.064391673
NLRX1	212.4509	221.9642	223.2164	40.54862	44.36439178	31.73340119
P2RX4	3.80714	2.219568	3.087093	0.544635	0.638353355	0.43965145
CACNA1H	0.134539	0.079275	0.095881	0.032984	0.008549837	0.016115913
ATP2A3	264.0552	264.1839	242.1261	51.74994	52.59420185	39.18563511
TBXA2R	0.431375	0.273731	0.401299	0.075929	0.067479236	0.063597093
TRADD	31.34045	31.47507	31.99384	5.943103	7.570489098	4.68749748
CAMK2D	6.316769	3.99198	4.792235	1.061932	0.981063853	0.931274309
ITPKC	1.510872	1.028177	1.422785	0.292157	0.324555827	0.173334172
CD274	0.218652	0.168047	0.206945	0.018645	0.02899845	0.072880381
IL17a	6.282759	5.792102	6.472462	28.19536	31.60670556	29.55617082
CXCL6	4.941397	4.744862	5.343573	0.897376	1.178547832	1.110744894
TFAM	8.876145	7.13092	7.85547	2.012327	2.01852259	1.21643535

ROCK2	2.690253	2.257855	2.845308	0.676593	0.570297169	0.499435241
PIN1	18.07414	17.21316	16.05014	4.191426	4.017837358	3.661108568
IL18	1.057252	0.788838	0.788838	7.698734	4.855093975	7.419699
MAPK11	1.056757	1.103021	0.907644	0.118437	0.368397975	0.231469134
RPS27	7.418937	5.401479	6.074088	1.73278	1.535564193	1.309735708
STAT1	15.27878	11.13477	12.22071	3.716867	3.07865959	2.634023471
RPS27A	5.807943	4.115433	4.368723	1.328978	1.150800973	1.084594337
FGFR2	6.223289	4.685365	5.369195	1.592069	1.381211003	1.116540523
TNF	23.02734	21.01244	19.44228	92.38244	69.70060853	81.25419099
CHD8	19.30457	14.57601	16.46314	4.913357	4.707668792	3.638549556
RPL31	0.195984	0.321739	0.223432	1.045047	0.701637555	0.90634069
MRPL2	13.71904	13.79403	13.67904	4.124498	3.823897539	3.806491594
MRPL4	10.76402	8.49893	9.851824	3.135708	3.038760875	2.323915934
SLC38A9	6.050901	4.422433	5.081207	1.640375	1.700800654	1.226606773
RPL12	0.925374	0.89502	0.681571	3.211137	2.348525302	2.803079575
USP8	4.031788	2.549237	3.385355	1.048297	0.958537379	0.984051831
ATM	0.6932	0.476207	0.647053	0.151423	0.203767315	0.192044394
RPS29	1.650417	1.025371	1.510388	0.440177	0.470434696	0.449987621
PTK2	20.61402	14.55238	17.78208	5.63733	6.053739167	5.588875293
LAMTOR3	5.485994	4.876636	5.417138	1.994272	1.695061057	1.506901922
CCL2	3.646499	2.689079	3.761401	1.127639	1.132783057	1.071900612
C2	37.87677	30.09844	27.87859	105.3703	90.30083618	93.26575542
F12	0.153902	0.135931	0.133681	0.476624	0.383588329	0.41574003
C8B	0.680404	0.451037	0.490487	1.888108	1.313589568	1.674238613

Supplementary figure legends

Supplementary figure S1:

(A) Representative IHC images showed GSDMD expression in HCC and adjacent nontumor tissues in two HCC cohorts.

(B) The GSDMD-FL and GSDMD-N expression in HCC cells.

(C) After the transfection of LV-control and LV-GSDMD-N in Huh7 cells and LV-shcontrol and LV-shGSDMD in MHCC97H cells, the GSDMD-N expression in HCC cells was shown.

(D) IL-1β and HMGB1 expression were exhibited by ELISA.

(E) IF revealed GSDMD expression in Huh7-control and Huh7-GSDMD-N cells.

Supplementary figure S2: Overexpression of GSDMD promotes hepatic tumorigenesis

(A) A schematic diagram for procedure of hepatocarcinogenesis in control and AAV9-FLEX-GSDMD-N groups treated by DEN and CCL_4.

(B) Representative H&E images were shown.

(C) Tumours numbers and maximal size of tumours from both groups.

(D) Quantification of proliferative hepatocytes or damaged livers of both genotypes at indicated time points.

(E) IF was used to exhibite αSMA staining.

(F) Correlation of *GSDMD* mRNA expression with mRNA expression of *Clo1a1* and *ACTA2* in non-tumour areas of hepatic tissues from control or AAV9-FLEX-GSDMD-N animals treated with DEN and CCl_4.

Supplementary figure S3: GSDMD deletion impairs hepatocarcinogenesis in mice treated with TAA.

(A) A schematic diagram for procedure of hepatocarcinogenesis in WT and GSDMD$^{-/-}$ mice induced by TAA.

(B) Liver tumours of both genotypes at indicated time points was shown by H&E images.

(C) Tumours number and maximal size of tumours from both groups.

(D) Quantification of proliferative hepatocytes or damaged livers of both genotypes at indicated time points.

(E) Masson and Sirius red staining exhibited collagenous fiber in two groups.

(F) IF was used to show αSMA staining in WT and *GSDMD*$^{-/-}$ group.

(G) Correlation of *GSDMD* mRNA expression with mRNA expression of *Clo1a1* and *ACTA2* in non-tumour areas of hepatic tissues from WT and *GSDMD*$^{-/-}$ group.

Supplementary figure S4: Intracellular K^+ is responsible for GSDMD-regulated IFNβ expression.

(A) Heatmaps showed variation analysis between WT and *GSDMD*$^{-/-}$ groups.

(B) Protein levels of IFN-β and TNFα was detected by ELISA in different groups.

(C) cGAMP level in indicated HCC cells as measured by UPLC/MS analysis.

(D) Relative cell vitality and IFN-β level were measured in Huh7-GSDMD-N cells with ploy(dA:dT) and/or glycine.

(E-F) IFN-β level was measured in different HCC groups.

(G) Relative cell vitality was measured in Huh7-GSDMD-N cells with ploy(dA:dT)

and/or KCL.

(H) IFN-β level was measured in Huh7-GSDMD cells with Pam3CSK4 and/or KCl.

Supplementary figure S5: cGAS inhibitor reverses GSDMD-KO-induced hepatic tumorigenesis

(A) Tumours number, maximal size and liver weight of tumours from both groups.

(B) The levels of ALT and AST were detected in different groups.

(C) Western blotting analyzed pSTING, STING, pTBK1, TBK1, pIRF3, IRF3 and β-actin in the mice of WT, GSDMD-/- and GSDMD-/-+cGAS inhibitor group.

(D) RT-qPCR analysis of indicated genes in liver tissues.

Supplementary figure S6:

(A) ChIP assays were used to illustrate binding of H3K27ac and H3K9ac on *CD274* promoter in HCC cells.

(B) Flow cytometry was applied to detect PD-L1 expression in three groups.

(C) Tumor volume was recorded in three groups.

(D) Tumor weight was exhibited in three groups.

(E) Ki67 staining was revealed.

(F) Western blotting showed expression of GSDMD-FL, RAGE, TLR2 and β-actin in indicated treatment cells.

Supplementary figure S7. GSDMD expression is positively associated with PD-L1 expression and negatively associated with pTBK1 expression in human HCC tissues.

(A) GSDMD, PD-L1 and pTBK1 expression in paired HCC tissues were performed by IHC staining.

(B) Correlation of IHC score between GSDMD and PD-L1 or pTBK1 expression was displayed in two HCC cohorts.

(C) The correlation between pTBK1 expression and recurrence and overall survival in two HCC cohorts was analyzed.

(D-E) The association of the co-expression of GSDMD and PD-L1 or pTBK1 with recurrent rate and overall survival time in two cohorts was assessed.

Supplementary figure S8. HMGB1 contributes to GSDMD-FL upregulation through TLR4/ERK/P65 pathway and cleaves GSDMD-FL through activating caspase-1

(A) Huh7 cells were treated with RhHMGB1 for 24 hours. GSDMD expression was detected by RT-qPCR.

(B) *GSDMD* promoter activity was detected after in Huhn7 cells treated with RhHMGB1.

(C) *GSDMD* promoter activity was examined in Huh7 cells transfected with plasmids of shcontrol or shP65 under HMGB1 treatment.

(D) RT-qPCR analysis of GSDMD mRNA in indicated HCC cells.

(E) ChIP assays showed binding of P65 on the *GSDMD* promoter.

(F) Tumor volume was recorded in three groups.

(G) Tumor weight was exhibited in three groups.

(H) Ki67 staining was revealed.

(I) TLR4, ERK, pERK and cGAS expression were detected with or without HMGB1 treatment.

(J) HMGB1, Cleaved Caspase-1, GSDMD, Pstat1, INF-β, and CD8 expression in HCC tissues were performed by IHC staining.

Supplementary figure S9. Combined GSDMD inhibitor DMF and PD-1 treatment

abolishes hepatic tumorigenesis and HCC metastasis.

(A) Schematic diagram of HCC mouse model.

(B) Total flux was recorded in mouse models.

(C) The levels of ALT, AST, Creatinine, and Blood urea nitrogen were detected in different groups.

(D) Overall survival time of C57BL/6 mice in different groups was shown.

(E) IF was applied to detect FOXP3 expression in liver tissues.

(F) IF was applied to illustrate CD11b expression in liver tissues.

(G) IFN-β was shown by ELISA.